

INVESTIGATION OF THE ATMOSPHERIC OZONE FORMATION POTENTIAL OF METHYL ACETATE

Report to
Eastman Chemical Company

by
William P. L. Carter, Dongmin Luo, and Irina L. Malkina

July 17, 1996

College of Engineering
Center for Environmental Research and Technology
University of California
Riverside, California 92521

ABSTRACT

A series of environmental chamber experiments and computer model calculations were carried out to assess the atmospheric ozone formation potential of methyl acetate. The experiments consisted of determining the effects of adding methyl acetate on NO oxidation, ozone formation and integrated OH radical levels in simulated model photochemical smog systems. Experiments were carried out using two different surrogate mixtures to represent the reactive organic gases (ROGs) present in the atmosphere, and using differing ROG/NO_x ratios. It was found that methyl acetate has a small but positive effect on ozone formation, and that it does not significantly enhance or inhibit OH radical levels. The results are well fit by model predictions if it assumes that methyl acetate reacts primarily to form a relatively unreactive product, with two NO to NO₂ being involved before OH radicals are regenerated. This suggests a mechanism involving formation of a $\cdot\text{CH}_2\text{O}(\text{CO})\text{CH}_3$ radical intermediate which primarily reacts with O₂ to form HO₂ and H(CO)O(CO)CH₃, though the latter product could not be detected by the analytical techniques we employed. The alternative mechanism, that the $\cdot\text{CH}_2\text{O}(\text{CO})\text{CH}_3$ radical decomposes to form formaldehyde and CO, significantly overpredicted the observed ozone impact of methyl acetate, and was inconsistent with the observation that the addition of methyl acetate had no significant effect on formaldehyde formation.

The experimentally-validated methyl acetate mechanism was then used to estimate its ozone impacts for a variety of atmospheric conditions. These were compared with ozone impacts calculated for ethane, the compound the EPA uses as the borderline for determining "negligible" ozone reactivity) and the mixture of all emitted VOCs. The results indicated that methyl acetate was approximately 1/3 to 1/2 as reactive as ethane, on an ozone per gram basis, with relatively little variation from scenario to scenario. Therefore, it is concluded that for regulatory purposes methyl acetate can be considered to have a lower ozone impact than that of ethane.

ACKNOWLEDGEMENTS

The authors gratefully acknowledge Mr. Dennis Fitz for assistance in administering this program, Mr. Kurt Bumiller and Ms. Kathalena Smihula for assistance in carrying out the experiments, and Dr. Roger Atkinson and Dr. David Morgott for helpful discussions. This work was funded by Eastman Chemical Co. However, the opinions and conclusions expressed in this report are entirely those of the primary author, Dr. William P. L. Carter. Mention of trade names or commercial products do not constitute endorsement or recommendation for use.

TABLE OF CONTENTS

<u>Section</u>	<u>Page</u>
LIST OF TABLES	iv
LIST OF FIGURES	iv
INTRODUCTION	1
EXPERIMENTAL AND DATA ANALYSIS METHODS	3
Overall Experimental Approach	3
Environmental Chamber	4
Experimental Procedures	4
Analytical Methods	5
Characterization Methods	6
Reactivity Data Analysis Methods	7
CHEMICAL MECHANISMS AND MODELING METHODS	9
General Atmospheric Photooxidation Mechanism	9
Atmospheric Reactions of Methyl Acetate	10
Environmental Chamber Simulations	11
Atmospheric Reactivity Simulations	12
RESULTS AND DISCUSSION	13
Summary of Experiments	13
Results of The Reactivity Experiments and Mechanism Evaluations	13
ATMOSPHERIC REACTIVITY CALCULATIONS	21
Scenarios Used for Reactivity Assessment	21
Base Case Scenarios	22
Adjusted NO _x scenarios	24
NO _x Conditions in the Base Case Scenarios	24
Incremental and Relative Reactivities	25
Reactivity Scales	26
Calculated Relative Reactivities of Methyl Acetate	27
CONCLUSIONS	29
REFERENCES	30
APPENDIX A. LISTING OF THE CHEMICAL MECHANISM	A-1

LIST OF TABLES

<u>Number</u>		<u>page</u>
1.	Chronological listing of all the chamber experiments carried out for this program.	14
2.	Summary of conditions and selected results of the incremental reactivity experiments. . . .	15
3.	Summary of conditions of base case scenarios used for atmospheric reactivity assessment.	23
4.	Summary of calculated incremental reactivities (gram basis) relative to ethane form methyl acetate, acetone, and the total of all emitted VOCs.	28
A-1.	List of species in the chemical mechanism used in the model simulations for this study.	A-1
A-2.	List of reactions in the chemical mechanism used in the model simulations for this study.	A-4
A-3.	Absorption cross sections and quantum yields for photolysis reactions.	A-9
A-4.	Values of chamber-dependent parameters used in the model simulations of the experiments for this study.	A-13

LIST OF FIGURES

<u>Number</u>		<u>page</u>
1.	Plots of selected results of the mini-surrogate + methyl acetate experiment DTC-336. . . .	16
2.	Plots of selected results of the mini-surrogate + methyl acetate experiment DTC-328. . . .	16
3.	Plots of selected results of the full surrogate + methyl acetate experiment DTC-327. . . .	17
4.	Plots of selected results of the full surrogate + methyl acetate experiment DTC-335. . . .	17
5.	Plots of selected results of the full surrogate + methyl acetate experiment DTC-332. . . .	18
6.	Plots of selected results of the low NO _x full surrogate + methyl acetate experiment DTC-329.	18
7.	Plots of selected results of the low NO _x full surrogate + methyl acetate experiment DTC-330.	19
8.	Experimental and calculated concentration-time plots for formaldehyde for all the reactivity experiments for which formaldehyde data are available.	20

INTRODUCTION

Ozone in photochemical smog is formed from the gas-phase reactions of volatile organic compounds (VOCs) and oxides of nitrogen (NO_x) in sunlight. Although Los Angeles has the worst ozone problem in the United States, other areas of the country also have episodes where ozone exceeds the federal air quality standard of 0.12 ppm. Ozone control strategies in the past have focused primarily on VOC controls, though the importance of NO_x control has become recognized in recent years. VOC and NO_x controls have differing effects on ozone formation. NO_x is required for ozone formation, and if the levels of NO_x are low compared to the levels of reactive VOCs, then changing VOC emissions will have relatively little effect on ozone. Since NO_x is removed from the atmosphere more rapidly than VOCs, ozone in areas far downwind from the primary sources tend to be more NO_x limited, and thus less responsive to VOC controls. VOC controls tend to reduce the rate that O_3 is formed when NO_x is present, so VOC controls are the most beneficial in reducing O_3 in the urban source areas, where NO_x is relatively plentiful, and where O_3 yields are determined primarily by how rapidly it is being formed. Because of this, any comprehensive ozone control strategy must involve reduction of emissions of both NO_x and VOCs.

Many different types of VOC compounds are emitted into the atmosphere, each reacting at different rates and having different mechanisms for their reactions. Because of this, they can differ significantly in their effects on ozone formation, or their "reactivity". Some compounds, such as CFCs, do not react in the lower atmosphere at all, and thus make no contribution to ground-level ozone formation. Others, such as methane, react and contribute to ozone formation, but react so slowly that their practical effect on ozone formation is negligible. Obviously, it does not make sense to regulate such compounds as ozone precursors. In recognition of this, the EPA has exempted certain compounds from such regulations on the basis of having "negligible" effects on ozone formation. Although the EPA has no formal policy on what constitutes "negligible" reactivity, in practice it has used the ozone formation potential of ethane as the standard in this regard. This is because ethane is the most reactive of the compounds that the EPA has exempted to date. Therefore, the ozone formation potential of a compound relative to ethane is of particular interest when assessing whether it might be a likely candidate for exemption from regulation as an ozone precursor.

Methyl acetate is a compound whose potential use as a solvent is of interest to Eastman Chemical Company. It is sufficiently volatile that its use might result in it being emitted into the atmosphere, and thus it would be subject to regulation as a VOC ozone precursor unless it can be shown to have negligible ozone reactivity. To assess this, Eastman Chemical asked us to review the information concerning the atmospheric chemistry and likely ozone reactivity of methyl acetate. The results of this assessment was that while there was no direct experimental information concerning its atmospheric ozone impact, and

there was a disagreement in the literature concerning the rate of its reaction in the atmosphere, it was likely that methyl acetate would have a very similar ozone impact as ethane. However, it was also concluded that at a minimum environmental chamber data are necessary to determine whether the estimated mechanism can reliably predict methyl acetate's effect on ozone, or to serve as a basis for deriving an alternative mechanism which can.

To improve the reliability of reactivity assessments of methyl acetate, Eastman Chemical Co. contracted the College of Engineering Center for Environmental Research and Technology (CE-CERT) to carry out the environmental chamber experiments to needed to provide an experimental basis to support the chemical mechanism used to calculate its atmospheric ozone impacts. The results of this program are documented in this report.

EXPERIMENTAL AND DATA ANALYSIS METHODS

Overall Experimental Approach

The environmental chamber experiments consisted primarily of measurements of "incremental reactivities" of methyl acetate under various conditions. These involve two types of irradiations of model photochemical smog mixtures. The first is a "base case" experiment where a mixture of reactive organic gases (ROGs) representing those present in polluted atmospheres (the "ROG surrogate") is irradiated in the presence of oxides of nitrogen (NO_x) in air. The second is the "test" experiment which consists of repeating the base case irradiation except that the VOC whose reactivity is being assessed is added. The differences between the results of these experiments provide a measure of the atmospheric impact of the test compound, and the difference relative to the amount added is a measure of its reactivity.

To provide data concerning the reactivities of the test compound under varying atmospheric conditions, three types of base case experiments were carried out:

1. Mini-Surrogate Experiments. This base case employed a simplified ROG surrogate and relatively low ROG/NO_x ratios. Low ROG/NO_x ratios represent "maximum incremental reactivity" (MIR) conditions, which are most sensitive to VOC effects. This is useful because it provides a sensitive test for the model, and also because it is most important that the model correctly predict a VOC's reactivity under conditions where the atmosphere is most sensitive to the VOCs. The ROG mini-surrogate mixture employed consisted of ethene, n-hexane, and m-xylene. This same surrogate was employed in our previous studies (Carter et al, 1993a,b; 1995a.), and was found to provide a more sensitive test of the mechanism than the more complex surrogates which more closely represent atmospheric conditions (Carter et al, 1995a). This high sensitivity to mechanistic differences makes the mini-surrogate experiments most useful for mechanism evaluation.

2. Full Surrogate Experiments. This base case employed a more complex ROG surrogate under somewhat higher, though still relatively low, ROG/NO_x conditions. While less sensitive to the mechanism employed, experiments with a more representative ROG surrogate are needed to evaluate the mechanism under conditions that more closely resembling the atmosphere. The ROG surrogate employed was the same as the 8-component "lumped molecule" surrogate as employed in our previous study (Carter et al., 1995a), and consists of n-butane, n-octane, ethene, propene, trans-2-butene, toluene, m-xylene, and formaldehyde. Calculations have indicated that use of this 8-component mixture will give essentially the same results in incremental reactivity experiments as actual ambient mixtures (Carter et al., 1995a).

3. Full Surrogate, low NO_x Experiments. This base case employing the same 8-component lumped molecule surrogate as the full surrogate experiments described above, except that lower NO_x levels (higher

ROG/NO_x ratios) were employed to represent NO_x-limited conditions. Such experiments are necessary to assess the ability of the model to properly simulate reactivities under conditions where NO_x is low. The initial ROG and NO_x reactant concentrations were comparable to those employed in our previous studies (Carter et al. 1995a).

An appropriate set of control and characterization experiments necessary for assuring data quality and characterizing the conditions of the runs for mechanism evaluation were also carried out. These are discussed where relevant in the results or modeling methods sections.

Environmental Chamber

The environmental chamber system employed in this study was the CE-CERT “Dividable Teflon Chamber” (DTC) with a blacklight light source. This consists of two ~5000-liter 2-mil heat-sealed FEP Teflon reaction bags located adjacent to each other and fitted inside an 8’x8’x8’ framework, and which uses two diametrically opposed banks of 32 Sylvania 40-W BL black lights as the light source. The lighting system in the DTC was found to provide so much intensity that only half the lights were used for irradiation. The unused black lights were covered with aluminum sheet as well, and were used to bring the chamber up to the temperature it will encounter during the irradiation before the uncovered lights are turned on. The air conditioner for the chamber room was turned on before and during the experiments. Four air blowers which are located in the bottom of the chamber were used to help cool the chamber as well as mix the contents of the chamber. The CE-CERT DTC is very similar to the SAPRC DTC which is described in detail elsewhere (Carter et al, 1995a,b).

The DTC is designed to allow simultaneous irradiations of the base case and the test experiments under the same reaction conditions. As indicated above, the chamber is actually two adjacent FEP Teflon reaction bags which can be simultaneously irradiated using the same light source and with the same temperature control system. These are referred to as the two “sides” of the chamber (Side A and Side B) in the subsequent discussion. The sides are interconnected with two ports, each with a box fan, which rapidly exchange their contents to assure that base case reactants have equal concentrations in both sides. In addition, a fan is located in each of the reaction bags to rapidly mix the reactants within each chamber. The ports connecting the two reactors can then be closed to allow separate injections on each side, and separate monitoring of each side. This design is optimized for carrying out incremental reactivity experiments such as those for this program.

Experimental Procedures

The reaction bags were flushed with dry air produced by an AADCO air purification system for 14 hours (6pm-8am) on the nights before experiments. The continuous monitors were connected prior to reactant injection and the data system began logging data from the continuous monitoring systems. The reactants were injected as described below (see also Carter et al, 1993b,, 1995b). The common reactants were injected in both sides simultaneously using a three-way (one inlet and two outlets connected to side

A and B respectively) bulb of 2 liters in the injection line and were well mixed before the chamber was divided. The contents of each side were blown into the other using two box fans located between them. Mixing fans were used to mix the reactants in the chamber during the injection period, but these were turned off prior to the irradiation. The sides were then separated by closing the ports which connected them, after turning all the fans off to allow their pressures to equalize. After that, reactants for specific sides (the test compound in the case of reactivity experiments) were injected and mixed. The irradiation began by turning on the lights and proceeded for 6 hours. After the run, the contents of the chamber were emptied by allowing the bag to collapse, and then was flushed with purified air. The contents of the reactors were vented into a fume hood.

The procedures for injecting the various types of reactants were as follows. The NO and NO₂ were prepared for injection using a high vacuum rack. Known pressure of NO, measured with MKS Baratron capacitance manometers, were expanded into Pyrex bulbs with known volumes, which were then filled with nitrogen (for NO) or oxygen (for NO₂). The contents of the bulbs were then flushed into the chamber with AADCO air. The other gas reactants were prepared for injection either using a high vacuum rack or a gas-tight syringes whose amounts were calculated. The gas reactants in a gas-tight syringe was usually diluted to 100-ml with nitrogen in a syringe. The volatile liquid reactants (including methyl acetate) were injected, using a micro syringe, into a 1-liter Pyrex bulb equipped with stopcocks on each end and a port for the injection of the liquid. The port was then closed and one end of the bulb was attached to the injection port of the chamber and the other to a dry air source. The stopcocks were then opened, and the contents of the bulb were flushed into the chamber with a combination of dry air and heat gun for approximately 5 minutes. Formaldehyde was prepared in a vacuum rack system by heating paraformaldehyde in an evacuated bulb until the pressure corresponded to the desired amount of formaldehyde. The bulb was then closed and detached from the vacuum system and its contents were flushed into the chamber with dry air through the injection port.

Analytical Methods

Ozone and nitrogen oxides (NO_x) were continuously monitored using commercially available continuous analyzers with Teflon sample lines inserted directly into the chambers. The sampling lines from each side of the chamber were connected to solenoids which switched from side to side every 10 minutes, so the instruments alternately collected data from each side. Ozone was monitored using a Dasibi 1003AH UV photometric ozone analyzer and NO and total oxides of nitrogen (including HNO₃ and organic nitrates) were monitored using a Teco Model 14B chemiluminescent NO/NO_x monitor. The output of these instruments, along with that from the temperature sensors and the and formaldehyde instrument, were attached to a computer data acquisition system, which recorded the data at 10 minutes intervals for ozone, NO and temperature (and at 15 minutes for formaldehyde), using 30 second averaging times. This yielded a sampling interval of 20 minutes for taking data from each side.

The Teco instrument and Dasibi CO analyzer were calibrated with a certified NO and CO source and CSI gas-phase dilution system. It was done prior to chamber experiment for each run. The NO₂ converter efficiency check was carried out in regular intervals. Dasibi ozone analyzer was calibrated against SAPRC transfer standard ozone analyzer using transfer standard method in a interval of three months and was check with CSI ozone generator (set to 400 ppb) for each experiment to assure that the instrument worked properly. The details were discussed elsewhere (Carter et al, 1995b)

Organic reactants other than formaldehyde were measured by gas chromatography with FID and ECD detections as described elsewhere (Carter et al., 1993b; 1995b). GC samples were taken for analysis at intervals from 20 minutes to 30 minutes either using 100 ml gas-tight glass syringes or by collecting the 100 ml sample from the chamber onto Tenax-GC solid adsorbent cartridge. These samples were taken from ports directly connected to the chamber after injection and before irradiation and at regular intervals after irradiation. Two sampling methods were employed for injecting the sample onto the GC column, depending on the volatility or "stickiness" of the compound. For analysis of the more volatile species (which includes all the components of the base case surrogates employed in this study), the contents of the syringe were flushed through a 2 ml or 3 ml stainless steel or 1/8' Teflon tube loop and subsequently injected onto the column by turning a gas sample valve.

The calibrations for the GC analyses for most compounds were carried out by sampling from chambers or vessels of known volume into which known amounts of the reactants were injected, as described previously (Carter et al, 1995b).

Characterization Methods

Three temperature thermocouples for each chamber were used to monitor the chamber temperature, two of which were located in the sampling line of continuous analyzers to monitor the temperature in each side. The third one was located in the chamber to monitor chamber temperature. The temperature in these experiment were typically 21-25 C for DTC and 25-30 C for CTC.

The light intensity in the DTC chamber was monitored by periodic NO₂ actinometry experiments utilizing the quartz tube method of Zafonte et al (1977), with the data analysis method modified as discussed by Carter et al. (1995b). The results of these experiments were tracked over time in this chamber since it was first constructed in early 1994, and were fit by a curve where the NO₂ photolysis rate decayed relatively rapidly from its initial values of ~0.31 min⁻¹ when the chamber and lights were new, then declining only slowly during the time of these experiments. A curve through the full set of actinometry results predicted NO₂ photolysis rates in the range of 0.216 - 0.217 min⁻¹ during the time of these experiments, and the results of the actinometry experiments associated with the runs in this study are consistent with this range. The spectrum of the blacklight light source was measured using a LiCor LI-1200 spectra radiometer, and found to be essentially the same as the general blacklight spectrum recommended by Carter et al (1995b) for use in modeling blacklight chamber experiments.

The dilution of the DTC chamber due to sampling is expected to be small because the flexible reaction bags can collapse as samples are withdrawn for analysis. However, some dilution occurs with the aging of reaction bags because of small leaks. Information concerning dilution in an experiment can be obtained from relative rates of decay of added VOCs which react with OH radicals with differing rate constants (Carter et al., 1993b; 1995b). Most experiments had a more reactive compounds such as m-xylene and n-octane present either as a reactant or added in trace amounts to monitor OH radical levels. Trace amounts (~0.1 ppm) of n-butane were also added to experiments if needed to provide a less reactive compound for monitoring dilution. In addition, specific dilution check experiments such as CO irradiations were carried out. Based on these results, the dilution rate was found to be 0.3% per hour in side A, and 0.1% per hour in side B.

Reactivity Data Analysis Methods

As indicated above, most of the experiments for this program consisted of simultaneous irradiation of a "base case" reactive organic gas (ROG) surrogate - NO_x mixture in one of the dual reaction chambers, together with an irradiation, in the other reactor, of the same mixture with a methyl acetate added. The results are analyzed to yield two measures of VOC reactivity: the effect of the added VOC on the amount of NO reacted plus the amount of ozone formed, and integrated OH radical levels. These are discussed in more detail below.

The first measure of reactivity is the effect of the VOC on the change in the quantity [O₃]-[NO], or ([O₃]_t-[NO]_t)-([O₃]₀-[NO]₀), which is abbreviated as d(O₃-NO) in the subsequent discussion. As discussed elsewhere (e.g., Johnson, 1983; Carter and Atkinson, 1987; Carter and Lurmann, 1990, 1991, Carter et al, 1993b, 1995b,c), this gives a direct measure of the amount of conversion of NO to NO₂ by peroxy radicals formed in the photooxidation reactions, which is the process that is directly responsible for ozone formation in the atmosphere. (Johnson calls it "smog produced" or "SP".) The incremental reactivity of the VOC relative to this quantity, which is calculated for each hour of the experiment, is given by

$$IR[d(O_3-NO)]_t^{VOC} = \frac{d(O_3-NO)_t^{test} - d(O_3-NO)_t^{base}}{[VOC]_0} \quad (1)$$

where d(O₃-NO)_t^{test} is the d(O₃-NO) measured at time t from the experiment where the test VOC was added, d(O₃-NO)_t^{base} is the corresponding value from the corresponding base case run, and [VOC]₀ is the amount of test VOC added. An estimated uncertainty for IR[d(O₃-NO)] is derived based on assuming an ~3% uncertainty or imprecision in the measured d(O₃-NO) values. This is consistent with the results of the side equivalency test, where equivalent base case mixtures are irradiated on each side of the chamber.

Note that reactivity relative to d(O₃-NO) is essentially the same as reactivity relative to O₃ in experiments where O₃ levels are high, because under such conditions [NO]_t^{base} ≈ [NO]_t^{test} ≈ 0, so a change d(O₃-NO) caused by the test compound is due to the change in O₃ alone. However, d(O₃-NO) reactivity

has the advantage that it provides a useful measure of the effect of the VOC on processes responsible for O₃ formation even in experiments where O₃ formation is suppressed by relatively high NO levels.

The second measure of reactivity is the effect of the VOC on integrated hydroxyl (OH) radical concentrations in the experiment, which is abbreviated as "IntOH" in the subsequent discussion. This is an important factor affecting reactivity because radical levels affect how rapidly all VOCs present, including the base ROG components, react to form ozone. If a compound is present in the experiment which reacts primarily with OH radicals, then the IntOH at time t can be estimated from

$$IntOH_t = \int_0^t [OH]_{\tau} d\tau = \frac{\ln\left(\frac{[tracer]_0}{[tracer]_t}\right) - Dt}{k_{OH}^{tracer}}, \quad (II)$$

where [tracer]₀ and [tracer]_t are the initial and time=t concentrations of the tracer compound, k_{OH}^{tracer} its OH rate constant, and D is the dilution rate in the experiments. The latter was found to be small and was neglected in our analysis. The concentration of tracer at each hourly interval was determined by linear interpolation of the experimentally measured values. m-Xylene was used as the OH tracer in these experiments because it is a surrogate component present in all experiments, its OH rate constant is known (the value used was 2.36x10⁻¹¹ cm³ molec⁻¹ s⁻¹ [Atkinson, 1989]), and it reacts relatively rapidly.

The effect of the VOC on OH radicals can thus be measured by its IntOH incremental reactivity, which is defined as

$$IR[IntOH]_t^{VOC} = \frac{IntOH_t^{test} - IntOH_t^{base}}{[VOC]_0} \quad (III)$$

where IntOH_t^{test} and IntOH_t^{base} are the IntOH values measured at time t in the added VOC and the base case experiment, respectively. The results are reported in units of 10⁶ min. The uncertainties in IntOH and IR[IntOH] are estimated based on assuming an ~2% imprecision in the measurements of the m-xylene concentrations. This is consistent with the observed precision of results of replicate analyses of this compound.

CHEMICAL MECHANISMS AND MODELING METHODS

General Atmospheric Photooxidation Mechanism

The chemical mechanism used in the environmental chamber and atmospheric model simulations in this study is given in Appendix A to this report. This mechanism is based on that documented by Carter (1990), with a number of updates as discussed below. It can explicitly represent a large number of different types of organic compounds, but it lumps together species reacting with similar rate constants and mechanisms in atmospheric simulations, and it uses a condensed representation for many of the reactive organic products. The reactions of inorganics, CO, formaldehyde, acetaldehyde, peroxyacetyl nitrate, propionaldehyde, peroxypropionyl nitrate, glyoxal and its PAN analog, methylglyoxal and several other product compounds are represented explicitly. In addition, the reactions of unknown photoreactive products formed in the reactions of aromatic hydrocarbons are represented by a model species "AFG2", whose yields and photolysis parameters are adjusted based on fits of model simulations to environmental chamber experiments. A chemical operator approach is used to represent peroxy radical reactions, as discussed in detail by Carter (1990). Generalized reactions with variable rate constants and product yields are used to represent the primary emitted alkane, alkene, aromatic and other VOCs (with rate constants and product yields appropriate for the individual compounds being represented in each simulation); The tables in the Appendix list only those VOCs (or groups of VOCs) used in the simulations in this work. Most of the higher molecular weight oxygenated product species are represented using the "surrogate species" approach, where simpler molecules such as propionaldehyde or 2-butanone are used to represent the reactions of higher molecular weight analogues that are assumed to react similarly.

Several aspects of the Carter (1990) mechanism were updated prior to this work to account for new kinetic and mechanistic information for certain classes of compounds as described by Carter et al. (1993a) and Carter (1995). In addition, further modifications were made to the uncertain portions of the mechanisms for the aromatic hydrocarbons to satisfactorily simulate results of experiments carried out using the chamber and light source employed in this study. The previously optimized aromatic mechanisms tended to underpredict the rates of NO oxidation and O₃ formation in the aromatic - NO_x experiments carried out in a chamber using a xenon arc light source (Carter et al, 1995c), so the aromatic mechanisms were reoptimized, by adjusting yields of model species used to represent uncharacterized ring-opening products (AFG2 and MGLY), to satisfactorily fit the chamber data. Note that while in the previous mechanisms the model species MGLY represented methylglyoxal alone, in the reoptimized mechanism it is being used to represent uncharacterized products as well. The reoptimized MGLY and AFG2 yields were for toluene were changed from respectively 0.13 and 0.49 to 0.85 and 0.27, and those for m-xylene were changed from 0.37 and 0.75 to 1.55 and 0.51, and the AFG2 photolysis rate was reduced by a factor of 2, relative to those used by the 1993 version of the mechanism (Carter et al, 1993a; Carter 1995). These updated aromatic mechanisms are still being developed, and a more detailed

discussion of them are beyond the scope of this paper. The reactions of methyl acetate are discussed in more detail below.

Atmospheric Reactions of Methyl Acetate

Methyl acetate is expected to react in the atmosphere primarily with OH radicals. Data in Calvert and Pitts (1977) indicates that this compound would not photolyze to a significant extent. Since ozone does not react to a significant extent with aldehydes and ketones (Atkinson and Carter, 1984), one would not expect ozone reaction with esters to be important. There are no data concerning the reactions of esters with NO₃ radicals, though, based on data for other compound and group-additivity methods, one would not expect the reactions to be rapid (Atkinson, 1991).

There is a discrepancy in the literature concerning the OH radical rate constant, with a measurement using a relative method giving a room temperature rate constant of $1.7 \times 10^{-13} \text{ cm}^3 \text{ molec}^{-1} \text{ s}^{-1}$ (Campbell and Parkinson, 1978), and a measurement using an absolute method yielding a rate constant expression of $0.83 \times 10^{-12} e^{-270/T} \text{ cm}^3 \text{ molec}^{-1} \text{ sec}^{-1}$ (Wallington et al., 1988), which gives a room temperature value of $3.4 \times 10^{-13} \text{ cm}^3 \text{ molec}^{-1} \text{ sec}^{-1}$, which is ~2 times higher. The relative method employed gave results for other compounds which were subsequently shown to be incorrect (Atkinson, 1989), so we consider the Wallington et al (1988) data more likely to be correct.

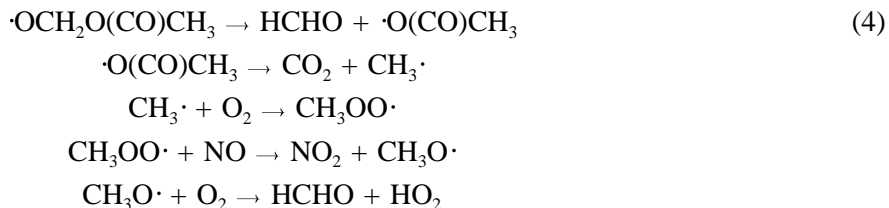
No published data are available concerning the mechanism and products of this reaction. Based on the structure-reactivity estimation methods (Atkinson, 1987), we expect most of the OH attack to occur at the OCH₃ end, with the initial reactions being as follows:



The relative importance of organic nitrate formation [reaction (3a)] compared to propagation forming the alkoxy radical [reaction (3b)] is uncertain, but, based on observed nitrate yields from lower molecular weight alkanes (Carter and Atkinson, 1989b) and computer modeling of chamber experiments with ethers (Carter et al, 1993b; Carter, 1995), one would expect the nitrate yield (k_{3a}/k_3) to be relatively low, and in absence of data to the contrary we assume it is negligible, i.e., that $k_{3a} \gg k_{3b}$. However, even a relatively low nitrate yield would have a non-negligible effect on reactivity (Carter, 1995), and this parameter could be adjusted if this assumption yields unsatisfactory fits of the model simulations to the results of the chamber experiments.

Another uncertainty is the subsequent reactions of the $\cdot\text{OCH}_2\text{O}(\text{CO})\text{CH}_3$ radical, which has two possible modes of reaction. In the initially estimated mechanism, we assumed that decomposition by

β -scission, which ultimately gives rise to two moles of formaldehyde and CO_2 and regenerating OH radicals after two NO to NO_2 conversions, dominates:



Assuming nitrate formation (reaction 3b) is unimportant, the overall process is thus:



This is referred to in the subsequent discussion as "Model A".

However, rate of the decomposition reaction (4) is uncertain, and an alternative process, reaction with O_2 may dominate over decomposition.



in which case the overall process (after reaction of HO_2 with NO regenerating OH) would be,



This alternative is referred to as "Model B" in the subsequent discussion.

Note that model B would predict lower O_3 formation potential for methyl acetate than Model A, both because it involves fewer NO to NO_2 conversions (the process ultimately responsible for ozone formation in these systems), and because formaldehyde would be expected to be much more reactive than $\text{H}(\text{CO})\text{O}(\text{CO})\text{CH}_3$. Based on structure-reactivity estimates (Atkinson, 1987) one would expect the latter product to react relatively slowly, and for simplicity in the model simulations using this mechanism it is represented by "MEK", which is used to represent other non-aldehyde oxygenated product species in the general mechanism (Carter, 1990).

Environmental Chamber Simulations

The ability of the chemical mechanisms to appropriately simulate the atmospheric impacts of methyl acetate was evaluated by conducting model simulations of the environmental chamber experiments from this study. This requires including in the model appropriate representations of chamber-dependent effects such as wall reactions and characteristics of the light source. The methods used are based on those discussed in detail by Carter and Lurmann (1990, 1991), updated as discussed by Carter et al (1995b,d). The photolysis rates were derived from results of NO_2 actinometry experiments and direct measurements of the spectra of the light source. In the case of the blacklights used in the DTC, the spectrum was assumed to be constant and the blacklight spectrum given by Carter et al (1995b,d) was employed. The thermal rate constants were calculated using the temperatures measured during the experiments, with the

small variations in temperature with time during the experiment being taken into account. The computer programs and modeling methods employed are discussed in more detail elsewhere (Carter et al, 1995b). The specific values of the chamber-dependent parameters used in the model simulations of the experiments for this study are given in Table 1. Both alternative methyl acetate models (A and B) were evaluated in the simulations of the chamber experiments.

Atmospheric Reactivity Simulations

To estimate its effects on ozone formation under conditions more representative of polluted urban atmospheres, incremental reactivities, defined as the change in O_3 caused by adding small amounts of a compound to the emissions, were calculated for ethane, methyl acetate, and several other representative compounds for various simulated atmospheric pollution scenarios. Carter (1994a) used a series of single-day EKMA box model scenarios (EPA, 1984) derived by the EPA to represent 39 different urban ozone exceedence areas around the United States (Baugues, 1990), to develop various reactivity scales to quantify impacts of VOCs on ozone formation in various environments. It was found that NO_x levels are the most important factor affecting differences in relative ozone impacts among VOCs, and that the ranges of relative reactivities in the various scales can be reasonably well represented by ranges in relative reactivities in three "averaged conditions" scenarios representing three different NO_x conditions. These scenarios were derived by averaging the inputs to the 39 EPA scenarios, except for the NO_x emissions. In the "maximum reactivity" scenario, the NO_x inputs were adjusted such that the final O_3 level is most sensitive to changes in VOC emissions; in the "maximum ozone" scenario the NO_x inputs were adjusted to yield the highest maximum O_3 concentration; and in the "equal benefit" scenario the NO_x inputs were adjusted such that relative changes in VOC and NO_x emissions had equal effect on ozone formation. As discussed by Carter (1994a), there represent respectively the high, medium and low ranges of NO_x conditions which are of relevance when assessing VOC control strategies for reducing ozone.

The chemical mechanisms used for these atmospheric simulations were the same as used to simulate the chamber experiments, except that the reactions representing chamber effects were removed, and the reactions for the full variety of VOCs emitted into the scenarios (Carter, 1994a) were represented (see Appendix A). Most of the emitted VOCs (other than the test compound whose reactivity is being calculated) are not represented in the model explicitly, but are represented using lumped model species whose rate constants and product yield parameters are derived based on the mixture of compounds they represent. The rate constants and mechanistic parameters for the emitted species in the scenarios were the same as those used previously (Carter, 1994a; Carter et al, 1993a), except for the aromatics, whose unknown photoreactive product yields were reoptimized in a manner analogous to that discussed above for toluene and m-xylene (unpublished results from this laboratory). The listings on Appendix A give the lumped model species used to represent the emissions into the scenarios, indicate the types of species each is used to represent, and give their rate constants and product yield parameters.

RESULTS AND DISCUSSION

Summary of Experiments

Table 1 gives a chronological listing of all the experiments carried out for this program. These consisted primarily of incremental reactivity experiments, whose conditions and selected results are summarized in more detail on Table 2. In addition, several characterization runs were carried out to determine the chamber-dependent inputs needed for the model simulations of the experiments. Control experiments were conducted to assure consistency with previous results, and side equivalency tests were conducted to assure that essentially equivalent results were obtained when equal mixtures were simultaneously irradiated in each of the dual reaction bags. Table 1 summarizes relevant results from these characterization and control runs.

The results of the characterization and control runs generally as expected based on our previous experience with these and similar chambers in our laboratories (Carter et al., 1995b and references therein). Good side equivalency was observed when equivalent surrogate - NO_x (not shown), propene - NO_x, CO - NO_x, or n-butane - NO_x (not shown) mixtures were simultaneously irradiated in the dual reactors. The results of the CO - NO_x experiments, which are highly sensitive to the magnitude of the chamber radical source assumed in the model (see Table A-4 in Appendix A), were sufficiently well simulated by the model to indicate that the model was appropriately representing this effect for these runs. The actinometry results agreed with the extrapolated values based on results of previous determinations (see Table A-4), to within the variability of these determinations.

Results of The Reactivity Experiments and Mechanism Evaluations

Summaries of the conditions and results of the incremental reactivity experiments are given on Table 2. Figures 1 through 7 give time series plots for relevant measurements used for mechanism evaluation. These include concentrations of d(O₃-NO) and m-xylene in the base case and test experiments, concentrations of the test alkane in the test experiment, and the d(O₃-NO) and IntOH incremental reactivities derived from the differences between the two sides. Results of model calculations, discussed below, are also shown in these figures. The dotted lines show the calculations using methyl acetate model "A", the solid lines show those for model "B", and the dashed lines show the base case calculations, which are the same for both models.

Table 2 shows that methyl acetate has a relatively low but still positive incremental reactivity with respect to d(O₃-NO), meaning that it is not an inhibitor of O₃ formation or NO oxidation. The effect of methyl acetate on integrated OH radicals under high NO_x conditions is extremely low, with the IntOH in the added methyl acetate sides being within the range of variability in the base case runs. Methyl acetate has a more negative effect on integrated OH radicals at the end of the low NO_x experiments, but

Table 1. Chronological listing of the environmental chamber experiments carried out for this program.

RunID	Date	Title	Comments
DTC322	3/4/96	CO - NOx	Control run to measure the chamber radical source. NO consumption rate well fit by predictions of the chamber model. CO consumption rate indicates relatively low dilution, but with dilution in Side A being somewhat greater than in side B
DTC326	3/11/96	NO2 Actinometry	Measured NO ₂ photolysis rate was 0.212 min ⁻¹ , in good agreement with the prediction of the curve fit to the full set of actinometry results through run 356, which was 0.217 min ⁻¹ ..
DTC327	3/22/96	Mini-surrogate + methyl acetate	
DTC328	3/28/96	Mini-surrogate + methyl acetate(B)	
DTC329	4/1/96	Full surrogate + methyl acetate (A)	No formaldehyde data
DTC330	4/2/96	Full surrogate + methyl acetate (B)	
DTC331	4/3/96	Propene - NOx	Control run for comparison with other propene runs carried out in this and other chambers. The model slightly overpredicted the ozone formation rate, but the results were within the normal range. Good side equivalency was observed.
DTC332	4/4/96	Full surrogate + methyl acetate (A) (higher NOx)	
DTC333	4/11/96	Pure air irradiation	After 6 hours of irradiation, approximately 31 ppb O ₃ formed on side A and 27 on side B. Results are within the normal range, and were consistent with the predictions of the chamber effects model.
DTC334	4/12/96	CO - NOx	NO consumption rate well fit by predictions of the chamber model. CO consumption rate indicates relatively low dilution, but with dilution in Side A being somewhat greater than in side B.
DTC335	4/16/96	Full surrogate + methyl acetate (B)	
DTC336	4/17/96	Mini surrogate + methyl acetate (A)	
DTC343	4/29/96	NO2 Actinometry	Measured NO ₂ photolysis rate was 0.209 min ⁻¹ , which is approximately 3% lower than the prediction of the curve fit to the full set of actinometry results through run 356, which was 0.216 min ⁻¹

Table 2. Summary of conditions and selected results of the incremental reactivity experiments.

this is attributable to the fact that enhancing the rate of O_3 formation under those conditions tends to reduce the overall radical levels at the end of the run. For example, similar negative IntOH reactivities have been observed in low NO_x experiments for carbon monoxide, a compound with a simple one-step mechanism converting OH to HO_2 , with no direct radical sources or sinks (Carter et al, 1995a). Thus these experiments indicate that methyl acetate does not have strong radical initiation or termination effects in its mechanism.

The results of the model simulations of the reactivity experiments are shown on Figures 1-7. The base case $d(O_3-NO)$ and m-xylene levels are simulated reasonably well, though the model may have a slight bias towards overpredicting $d(O_3-NO)$ formation rates. Model B performs quite well in simulating the effect of methyl acetate addition on both $d(O_3-NO)$ and IntOH, while model A performs poorly, consistently predicting a much larger effect of methyl acetate on $d(O_3-NO)$ than is observed experimentally. Both models predict similar effects on IntOH, but the differences in effects on $d(O_3-NO)$ are significant.

Note that the difference between models A and B are that the former predicts formation of two moles of formaldehyde for each mole of methyl acetate reacting, while the latter predicts formation of a relatively inert product, and Model A predicts that one more NO to NO_2 conversion is involved in methyl acetate's photooxidation than does Model B. It is the additional NO to NO_2 conversion, the process ultimately responsible for O_3 formation, which is the primary reason that Model A predicts the higher $d(O_3-NO)$ reactivity. The relatively high reactivity of formaldehyde is also a factor, and is the reason that Model A predicts higher IntOH reactivities than does model B. However, the differences

Table 2. Summary of conditions and results of the incremental reactivity experiments.

Run	Initial Reactants (ppm)			t=6 d(O ₃ -NO) (ppm)			t=6 IntOH (10 ⁶ min)		
	NOx	Surg [a]	Me.Acet.	Base	Test	IR [b]	Base	Test	IR
Mini-Surrogate									
DTC-336 (A)	0.31	5.2	21.1	0.57	0.69	0.0055	18	18	0.0
DTC-328 (B)	0.32	5.6	15.2	0.56	0.66	0.0067	19	17	-0.2
Full Surrogate - High NOx									
DTC-327 (A)	0.33	5.5	9.8	0.60	0.67	0.0077	19	21	0.2
DTC-335 (B)	0.41	3.9	11.0	0.46	0.57	0.0099	22	21	-0.1
DTC-332 (A)	0.58	3.7	12.0	0.37	0.46	0.0071	16	16	0.0
Full Surrogate - Low NOx									
DTC-329 (A)	0.17	3.8	18.1	0.49	0.59	0.0059	31	28	-0.1
DTC-330 (B)	0.17	3.9	11.9	0.48	0.58	0.0088	32	27	-0.4

Notes

[a] Total base ROG surrogate in ppmC.

[b] Incremental reactivity

DTC336A: 21.1 ppm ME-ACET

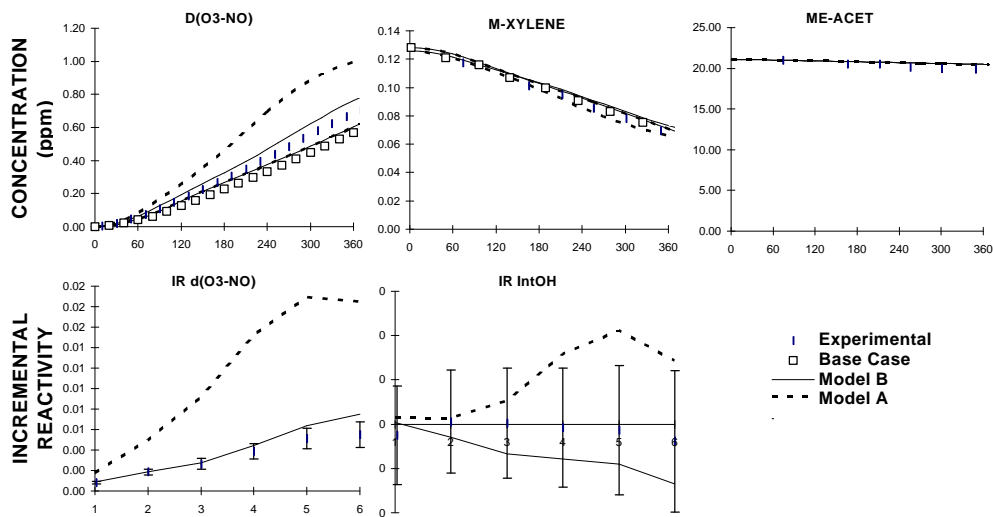


Figure 1. Plots of selected results of the mini-surrogate + methyl acetate experiment DTC-336.

DTC328B: 15.2 ppm ME-ACET

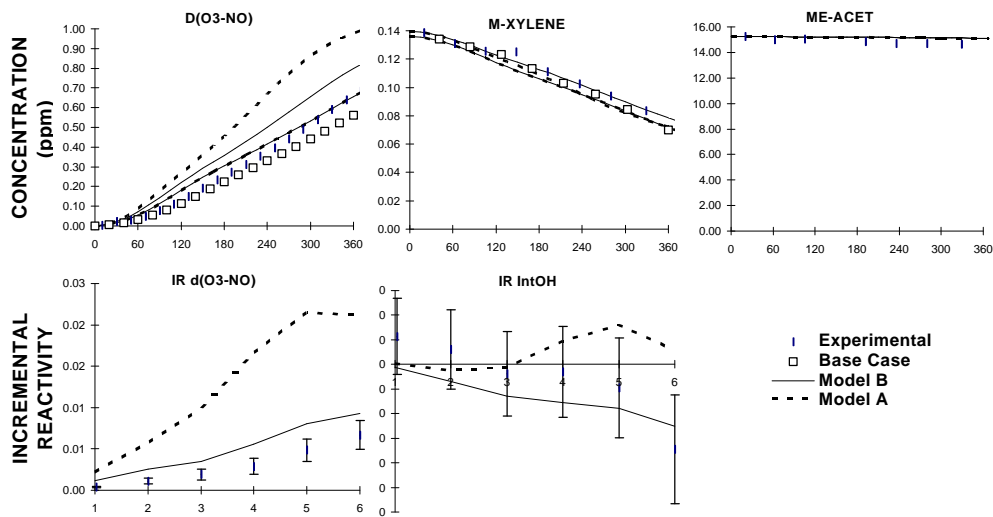


Figure 2. Plots of selected results of the mini-surrogate + methyl acetate experiment DTC-328.

DTC327A: 9.8 ppm ME-ACET

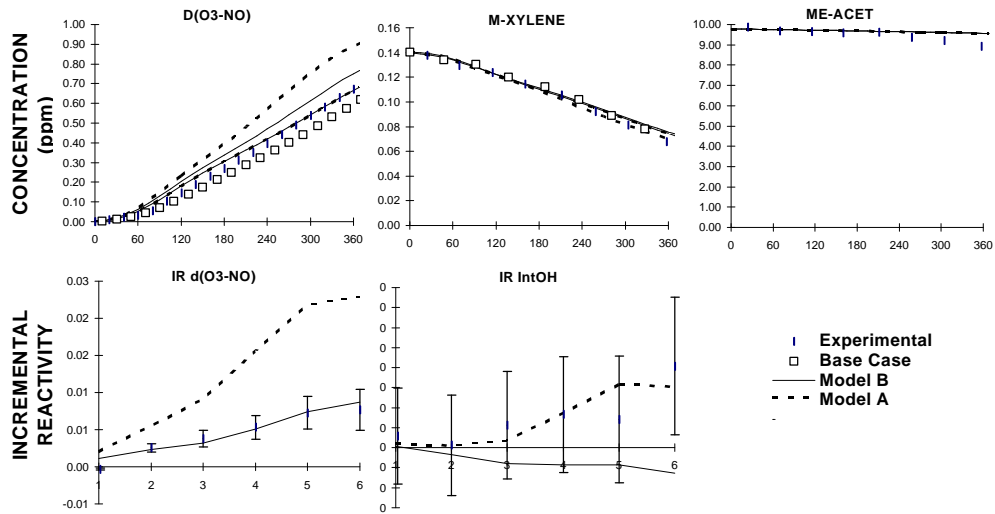


Figure 3. Plots of selected results of the full surrogate + methyl acetate experiment DTC-327.

DTC335B: 11.0 ppm ME-ACET

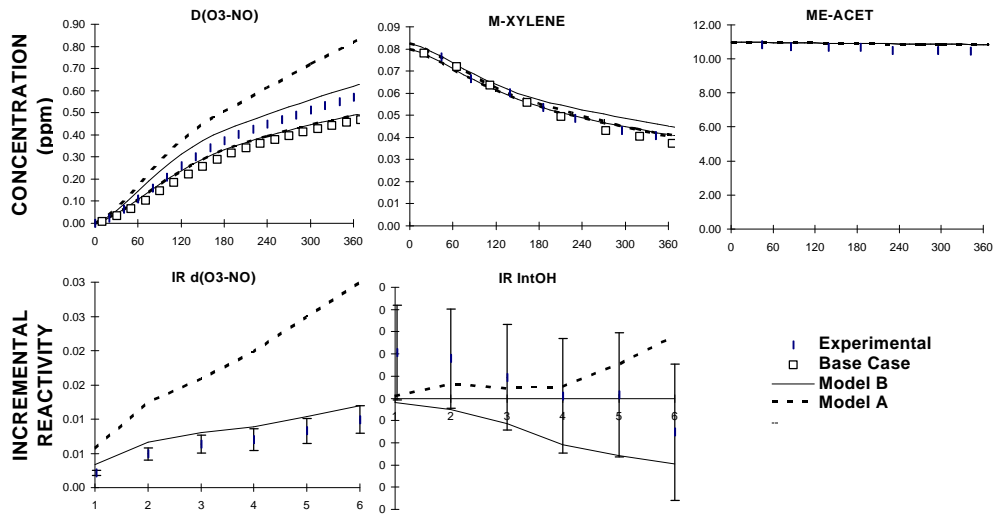


Figure 4. Plots of selected results of the full surrogate + methyl acetate experiment DTC-335.

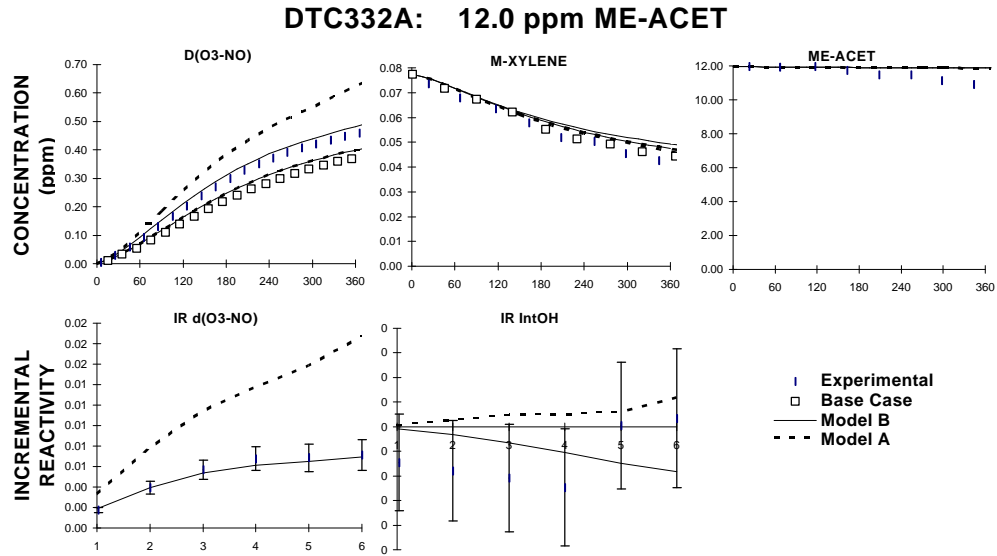


Figure 5. Plots of selected results of the full surrogate + methyl acetate experiment DTC-332.

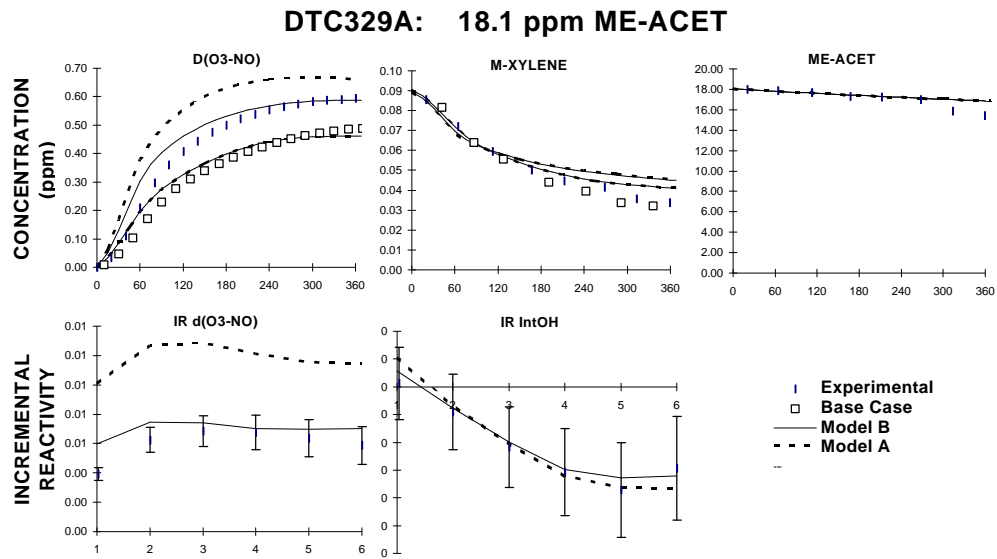


Figure 6. Plots of selected results of the low NO_x full surrogate + methyl acetate experiment DTC-329.

Figure 7. Plots of selected results of the low NO_x full surrogate + methyl acetate experiment DTC-330.

between the models in their IntOH predictions are not outside experimental uncertainty, so the IntOH data by themselves are not useful for distinguishing between these models.

Additional evidence against Model A comes from comparing the experimental and calculated formaldehyde data for these experiments, which are shown on Figure 8. It can be seen that essentially the same amount of formaldehyde is formed on the side of the experiments where the methyl acetate is added as on the base case side, indicating that it is not formed to a significant extent from methyl acetate. The predictions of Model B, which assumes that formaldehyde is not formed, is consistent with this. On the other hand, Model A predicts that approximately twice as much formaldehyde should be formed on the added methyl acetate side as in the base case runs, a difference which is far outside the experimental uncertainty or variability.

DTC330B: 11.9 ppm ME-ACET

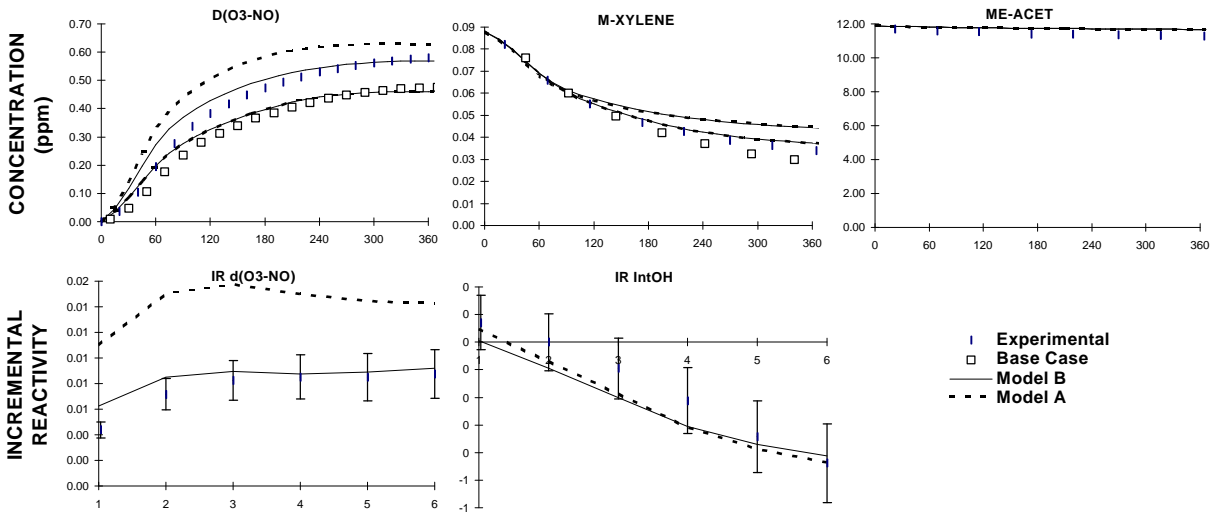
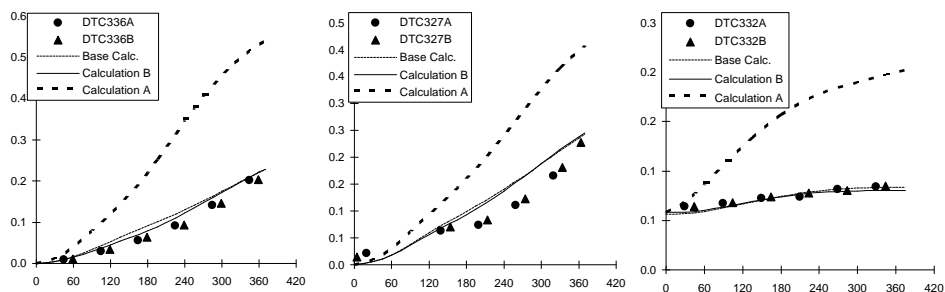


Figure 7. Plots of selected results of the low NO_x full surrogate + methyl acetate experiment DTC-330.

TC-336 (A) (MINI-SURROGAT C-327 (A) (FULL SURROGAT C-332 (A) (FULL SURROGAT



TC-328 (B) (MINI-SURROGAT C-335 (B) (FULL SURROGAT DTC-330 (B) (LOW NO_x)

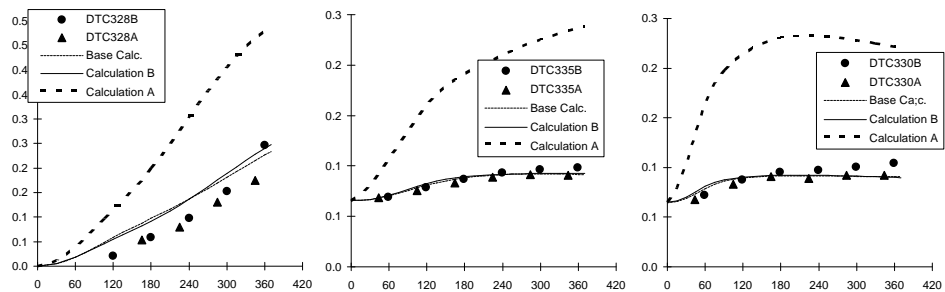


Figure 8. Experimental and calculated concentration-time plots for formaldehyde for all the reactivity experiments for which formaldehyde data are available

ATMOSPHERIC REACTIVITY CALCULATIONS

Incremental reactivities of VOCs have been shown to be highly dependent on environmental conditions, so reactivities measured in environmental chamber experiments cannot necessarily be assumed to be exactly the same as those under atmospheric conditions (Carter and Atkinson, 1989a; Carter et al, 1995a). The only method available to obtain quantitative estimates of incremental reactivities of VOCs in ambient air pollution episodes is to conduct airshed model simulations of the episodes. Since these simulations cannot be any more reliable than the chemical mechanisms used, the major objective of this program was to assess the reliability of the methyl acetate mechanism for use in such simulations. This was discussed in the previous sections. In this section, we discuss the results of model simulations of its incremental reactivities in a variety of model scenarios representing ozone exceedence episodes in various areas in the United States (Baugues, 1990), and compare the results to incremental reactivities calculated for ethane, the compound used by the EPA as the criterion for determining "negligible" reactivity, and for the base ROG, the mixture representing total ROG emissions from all sources. Because the data from these experiments tend to validate model "B" and rule out model "A", only model "B" is used in the atmospheric reactivity calculations for methyl acetate.

Scenarios Used for Reactivity Assessment

The set of airshed scenarios employed to assess the methyl acetate reactivity for this study is the same as those used for calculating the MIR and other reactivity scales (Carter, 1994a; Carter et al, 1993a). The objective is to use a set of scenarios which represents, as much as possible, a comprehensive distribution of the environmental conditions where unacceptable levels of ozone are formed. Although a set of scenarios has not been developed for the specific purpose of VOC reactivity assessment, the EPA developed an extensive set of scenarios for conducting analyses of effects of ROG and NO_x controls on ozone formation using the EKMA modeling approach (Gipson et al., 1981; Gipson and Freas, 1983; EPA, 1984; Gery et al., 1987; Baugues, 1990). The EKMA approach involves the use of single-cell box models to simulate how the ozone formation in one day episodes is affected by changes in ROG and NO_x inputs. Although single-cell models cannot represent realistic pollution episodes in great detail, they can represent dynamic injection of pollutants, time-varying changes of inversion heights, entrainment of pollutants from aloft as the inversion height raises, and time-varying photolysis rates, temperatures, and humidities (Gipson and Freas, 1981; EPA, 1984; Gipson, 1984; Hogo and Gery, 1988). Thus, they can be used to simulate a wide range of the chemical conditions which affect ozone formation from ROG and NO_x, and which affect VOC reactivity. Therefore, at least to the extent they are suitable for their intended purpose, an appropriate set of EKMA scenarios should also be suitable for assessing reactivities over a wide range of conditions.

Base Case Scenarios

The set of EKMA scenarios used in this study were developed by the United States EPA for assessing how various ROG and NO_x control strategies would affect ozone nonattainment in various areas of the country (Baugues, 1990). The characteristics of these scenarios and the methods used to derive their input data are described in more detail elsewhere (Baugues, 1990; Carter, 1993). Briefly, 39 urban areas in the United States were selected based on geographical representativeness of ozone nonattainment areas and data availability, and a representative high ozone episode was selected for each. The initial NMOC and NO_x concentrations, the aloft O₃ concentrations, and the mixing height inputs were based on measurement data for the various areas, the hourly emissions in the scenarios were obtained from the National Acid Precipitation Assessment Program emissions inventory (Baugues, 1990), and biogenic emissions were also included. Table 3 gives a summary of the urban areas represented and other selected characteristics of the scenarios.

Several changes to the scenario inputs were made based on discussions with the California ARB staff and others (Carter, 1993). Two percent of the initial NO_x and 0.1% of the emitted NO_x in all the scenarios was assumed to be in the form of HONO. The photolysis rates were calculated using solar light intensities and spectra calculated by Jeffries (1991) for 640 meters, the approximate mid-point of the mixed layer during daylight hours. The composition of the NMOCs entrained from aloft was based on the analysis of Jeffries et al (1989). The composition of the initial and emitted reactive organics was derived as discussed below. Complete listings of the input data for the scenarios are given elsewhere (Carter, 1993).

This set of 39 EKMA scenarios are referred to as "base case" to distinguish them from the scenarios derived from them by adjusting NO_x inputs to yield standard conditions of NO_x availability as discussed below. No claim is made as to the accuracy of these scenarios in representing any real episode, but they are a result of an effort to represent, as accurately as possible given the available data and the limitations of the formulation of the EKMA model, the range of conditions occurring in urban areas throughout the United States. When developing general reactivity scales it is more important that the scenarios employed represent a realistic distribution of chemical conditions than accurately representing the details of any one particular episode.

The Base ROG mixture is the mixture of reactive organic gases used to represent the chemical composition of the initial and emitted anthropogenic reactive organic gases from all sources in the scenarios. Consistent with the approach used in the original EPA scenarios, the same mixture was used for all scenarios. The speciation for this mixture was derived by Croes (1991) based on an analysis of the EPA database (Jeffries et al. 1989) for the hydrocarbons and the 1987 Southern California Air Quality Study (SCAQS) database for the oxygenates (Croes et al., 1994; Lurmann et al., 1992). This mixture consists of 52% (by carbon) alkanes, 15% alkenes, 27% aromatics, 1% formaldehyde, 2% higher

Table 3. Summary of conditions of base case scenarios used for atmospheric reactivity assessment.

City, State	Calc. Max O ₃ (ppb)	ROG /NO _x	NO _x /NO _x ^{MOR}	Final Height (km)	Init.+Emit Base ROG (mmol m ⁻²)	Aloft O ₃ (ppb)
Atlanta, GA	174	7.3	0.7	2.1	12	63
Austin, TX	171	9.3	0.5	2.1	11	85
Baltimore, MD	304	5.2	1.1	1.2	17	84
Baton Rouge, LA	235	6.8	1.0	1.0	11	62
Birmingham, AL	233	6.9	0.6	1.8	13	81
Boston, MA	191	6.5	0.6	2.6	14	105
Charlotte, NC	142	7.8	0.3	3.0	7	92
Chicago, IL	273	11.6	0.5	1.4	25	40
Cincinnati, OH	192	6.4	0.8	2.8	17	70
Cleveland, OH	239	6.6	1.0	1.7	16	89
Dallas, TX	192	4.7	1.3	2.3	18	75
Denver, CO	195	6.3	1.2	3.4	29	57
Detroit, MI	229	6.8	0.8	1.8	17	68
El Paso, TX	177	6.6	1.1	2.0	12	65
Hartford, CT	166	8.4	0.5	2.3	11	78
Houston, TX	291	6.1	1.0	1.7	25	65
Indianapolis, IN	201	6.6	0.9	1.7	12	52
Jacksonville, FL	152	7.6	0.7	1.5	8	40
Kansas City, MO	151	7.1	0.6	2.2	9	65
Lake Charles, LA	282	7.4	0.7	0.5	7	40
Los Angeles, CA	546	7.6	1.0	0.5	23	100
Louisville, KY	203	5.5	0.9	2.5	14	75
Memphis, TN	218	6.8	0.7	1.8	15	58
Miami, FL	131	9.6	0.4	2.7	9	57
Nashville, TN	163	8.1	0.5	1.6	7	50
New York, NY	350	8.1	0.8	1.5	39	103
Philadelphia, PA	230	6.2	1.0	1.8	19	53
Phoenix, AZ	258	7.6	1.0	3.3	40	60
Portland, OR	161	6.5	0.7	1.6	6	66
Richmond, VA	225	6.2	0.8	1.9	16	64
Sacramento, CA	194	6.6	0.9	1.1	7	60
St Louis, MO	301	6.1	1.1	1.6	26	82
Salt Lake City, UT	179	8.5	0.6	2.2	11	85
San Antonio, TX	126	3.9	1.1	2.3	6	60
San Diego, CA	186	7.1	1.0	0.9	8	90
San Francisco, CA	222	4.8	1.8	0.7	25	70
Tampa, FL	217	4.4	1.1	1.0	8	68
Tulsa, OK	216	5.3	0.9	1.8	15	70
Washington, DC	268	5.3	0.9	1.4	13	99

aldehydes, 1% ketones, and 2% acetylene. The detailed composition of this mixture is given elsewhere (Carter, 1993).

Adjusted NO_x scenarios

Incremental reactivities in the base case scenarios would be expected to vary widely, since incremental reactivities depend on the ROG/NO_x ratio, and that ratio varies widely among the base case scenarios. To obtain reactivity scales for specified NO_x conditions, separate sets of scenarios, designated MIR (for maximum incremental reactivity), MOR (for maximum ozone reactivity), and Equal Benefit Incremental Reactivity (EBIR) were developed (Carter, 1984). In the MIR scenarios, the NO_x inputs were adjusted so the base ROG mixture (and most other VOCs) have their highest incremental reactivity. This is representative of the highest NO_x conditions of relevance to VOC reactivity assessment because at higher NO_x levels O₃ yields become significantly suppressed, but is also the condition where O₃ is most sensitive to VOC emissions. In the MOR scenarios, the NO_x inputs were adjusted to yield the highest ozone concentration. In the EBIR scenarios, the NO_x inputs were adjusted so that the relative effects of NO_x reductions and total ROG reductions on peak ozone levels were equal. This represents the lowest NO_x condition of relevance for VOC reactivity assessment, because O₃ formation becomes more sensitive to NO_x emissions than VOC emissions at lower NO_x levels. The changes in the base case ROG/NO_x ratios which yielded the MOR scenarios are given in Table 3. As discussed by Carter (1994a) the MIR and EBIR ROG/NO_x ratios are respectively ~1.5 and ~0.7 times those for the MOR scenarios in all cases.

For this study, the MIR, MOIR, and EBIR reactivities were calculated using the "averaged conditions" scenarios with the corresponding adjusted NO_x conditions. As discussed by Carter (1994a), averaged conditions scenarios have all inputs derived by averaging the corresponding inputs of the base case scenarios, except that the NO_x inputs were adjusted to yield the specified NO_x conditions as discussed above. This is slightly different than the approach used by Carter (1994a) to derive the MIR, MOIR, and EBIR scales, which involved adjusting NO_x conditions separately for each of the 39 base case scenarios, and then averaging the reactivities derived from them. Since Carter (1994a) showed that both approaches yield essentially the same result. For this work use of the averaged conditions approach was preferred because it is computationally much more straightforward, and gives an equally a good indication of how the relative reactivities of compounds vary with varying NO_x conditions.

NO_x Conditions in the Base Case Scenarios

The variability of ROG/NO_x ratios in the base case scenarios suggest a variability of reactivity characteristics in the base case scenarios. However, as discussed previously (Carter, 1994a), the ROG/NO_x ratio is also variable in the MIR or MOR scenarios, despite the fact that the NO_x inputs in these scenarios are adjusted to yield a specified reactivity characteristic. Thus, the ROG/NO_x ratio, by itself, is not necessarily a good predictor of reactivity characteristics of a particular scenario. The NO_x/NO_x^{MOR} ratio is a much better predictor of this, with values greater than 1 indicating relatively high NO_x conditions where ozone formation is more sensitive to VOCs, and values less than 1 indicating NO_x-limited

conditions. $\text{NO}_x/\text{NO}_x^{\text{MOR}}$ ratios less than 0.7 represent conditions where NO_x control is a more effective ozone control strategy than ROG control (Carter, 1994a). Note that more than half of the base case scenarios represent NO_x -limited conditions, and ~25% of them represent conditions where NO_x control is more beneficial than VOC control. A relatively small number of scenarios represent MIR or near MIR conditions. However, as discussed elsewhere (Carter, 1994a), this set of scenarios is based on near-worst-case conditions for ozone formation in each of the airsheds. Had scenarios representing less-than-worst-case conditions been included, one might expect a larger number of MIR or near MIR scenarios. This is because NO_x is consumed more slowly on days with lower light intensity or temperature, and thus the scenario is less likely to become NO_x -limited.

Incremental and Relative Reactivities

The incremental reactivity of a VOC in an airshed scenario is the change in ozone caused by adding the VOC to the emissions, divided by the amount of VOC added, calculated for sufficiently small amounts of added VOC that the incremental reactivity is independent of the amount added. The procedure used to calculate incremental reactivities in a scenario was as discussed in detail elsewhere (Carter, 1993, 1994a,b). The incremental reactivities depend on how the amount of VOC added are quantified. In this work, the added VOC was quantified on a mass basis, since this is how VOCs are regulated. In addition, the incremental reactivities also depend on how ozone impacts are quantified (Carter, 1994a). In this work, two different ozone quantifications were used, resulting in two different incremental reactivities being calculated for a VOC in a scenario. These are discussed below.

The "Ozone Yield" incremental reactivities measure the effect of the VOC on the total amount of ozone formed in the scenario at the time of its maximum concentration. In this work, this is quantified as grams O_3 formed per gram VOC added. This gives the same ratios of incremental reactivities as reactivities calculated from peak ozone concentrations, but is preferred because it permits magnitudes of reactivities in scenarios with differing dilutions to be compared on the same basis. Most previous recent studies of incremental reactivity (Dodge, 1984; Carter and Atkinson, 1987, 1989a, Chang and Rudy, 1990; Jeffries and Crouse, 1991) have all been based on ozone yield or peak ozone concentration reactivities.

The ozone yield incremental reactivities do not necessarily measure the effect of the VOC on exposure to unacceptable levels of ozone because it does not measure how long high levels of ozone are present. A quantification which reflects this is integrated ozone over the standard, which is defined as the sum of the hourly ozone concentrations for the hours when ozone exceeds the standard in the base case scenarios (Carter 1994a). In the previous work (Carter, 1994a), we used the California ozone standard of 90 ppb, but in this work we will use the national standard of 0.12 ppm. Reactivities relative to this quantification of ozone are referred to by the abbreviation "Int $\text{O}_3 > 0.12$ " reactivities.

Relative reactivities are ratios of incremental reactivities to incremental reactivities of some standard VOC or mixture. Since these are the quantities which usually are the most relevant to control

strategy applications, the results in this work will be given in terms of relative reactivities. In our previous work (Carter 1991, 1994a), we used the incremental reactivity of the base ROG mixture, i.e., the mixture representing ROG pollutants from all sources, as the standard to define relative reactivities. However, because of the tendency within the EPA to consider ethane as the standard to define exempt vs controlled VOCs, in this work we will present reactivity ratios where ethane is used as the standard.

Reactivity Scales

A reactivity scale is a set of incremental or relative reactivities for a particular scenario or group of scenarios. Two types of reactivity scales will be discussed here, "base case" scales and adjusted NO_x scales. Base case scales are simply the set of incremental or relative reactivities in the 39 base case scenarios. Two sets of base case scales are derived — those based ozone yield reactivities and those based on IntO₃>0.12 reactivities. In the previous work (Carter, 1991, 1994a) we derived various multi-scenario scales from the individual base case scales by averaging or other procedures, to evaluate alternative approaches for developing single reactivity scales for applications requiring single scales. However, the decision of whether to exempt a VOC should not be made based on relative reactivities of a single scale, but on a knowledge of the range of relative reactivities for a variety of conditions. Thus in this work we present the distribution of base case relative reactivities for the 39 individual scenarios rather than developing aggregated or optimum scales which represent the distribution by single numbers.

The adjusted NO_x incremental reactivity scales refer to the MIR (maximum incremental reactivity), MOIR (maximum ozone incremental reactivity), or the EBIR (Equal Benefit Incremental Reactivity) scales. In this work, these consist of ozone yield incremental reactivities in averaged conditions scenarios where NO_x inputs were adjusted to yield MIR, MOR or EBIR conditions, respectively. Relative reactivities in these scales are ratios of incremental reactivities in these scales. Reactivities in the MIR scale are of interest because the California Air Resources Board utilized an MIR scale to calculate reactivity adjustment factors in its clean fuels/low emissions vehicle regulations (CARB, 1993). The justification for using this scale in applications requiring a single scale (such as the CARB vehicle regulations) is that it reflects conditions where ozone is most sensitive to changes in VOC emissions, and complements NO_x control, which is most effective for reducing ozone under conditions where the MIR scale is least applicable (Carter, 1994a). The MOIR scale is preferred by many as an alternative for such applications because it reflects conditions which are most favorable for ozone, and is more representative of the distribution of conditions in the base case scenarios (Carter 1994a). Most other alternative reactivity scales which might be appropriate for assessing VOC control strategies (i.e., excluding scales representing highly NO_x-limited conditions where ozone is more sensitive to NO_x than VOCs) tend to fall in the range defined by the MIR and MOIR scales. Since the EBIR scale represents lower NO_x conditions where O₃ is less sensitive to VOCs, its use in applications requiring a single scale has not been considered. However, it is useful for assessing how reactivities depend on NO_x conditions.

Note that the MIR, MOIR, EBIR and base case scales derived in this work are somewhat different from those calculated previously (Carter, 1994a; Carter et al, 1993a) because an updated chemical mechanism was used. The updates to the mechanism were discussed in the previous section. In addition, as indicated above, for computational efficiency the MIR, MOIR and EBIR scales were calculated using a single averaged conditions scenario, rather than the average of the adjusted NO_x base case scenarios as done previously (Carter, 1994a).

Calculated Relative Reactivities of Methyl Acetate

Table 4 lists the ozone yield and IntO₃>0.12 reactivities methyl acetate relative to ethane and relative to the total of all emitted VOCs for the base case and the adjusted NO_x averaged conditions scenarios. It can be seen that methyl acetate is calculated to be between ~30% and ~50% as reactive as ethane for all scenarios and for both ozone quantification methods. There is no scenario in which methyl acetate is more reactive than ethane, with the maximum reactivity ratios for the ozone yield or IntO₃>0.12 quantification methods being 61% and 58%, respectively. Methyl acetate is between 3% and 10% as reactive as the total of all VOC emissions (the base ROG), with its reactivity relative to the base ROG being somewhat lower if the integrated ozone quantification method is used.

Table 4. Summary of calculated relative incremental reactivities (gram basis) for methy acetate, ethane, and the total of all emitted VOCs.

Scenario	Relative to the Total of Emitted VOCS (Base ROG)				Relative to Ethane			
	O ₃ Yield Reactivity		IntO ₃ >0.12 Reactivity		O ₃ Yield Reactivity		IntO ₃ >0.12 Reactivity	
	Me-Acet.	Ethane	Me-Acet.	Ethane	Me-Acet.	Base ROG	Me-Acet.	Base ROG
<u>Averaged Conditions</u>								
Max React	0.025	0.077	0.023	0.070	0.32	12.94	0.33	14.20
Max Ozone	0.055	0.148	0.037	0.097	0.37	6.75	0.38	10.29
Equal Benefit	0.076	0.190	0.023	0.070	0.40	5.26	0.33	14.20
<u>Base Case</u>								
Average	0.069	0.172	0.049	0.116	0.40	6.28	0.42	9.21
St.Dev	29%	24%	31%	26%	0.12	0.38	0.13	0.30
ATL GA	0.067	0.167	0.052	0.119	0.40	5.98	0.44	8.39
AUS TX	0.077	0.193	0.063	0.136	0.40	5.17	0.46	7.34
BAL MD	0.056	0.152	0.032	0.086	0.37	6.57	0.37	11.59
BAT LA	0.066	0.152	0.047	0.101	0.43	6.59	0.47	9.86
BIR AL	0.087	0.233	0.053	0.131	0.37	4.28	0.40	7.63
BOS MA	0.083	0.204	0.053	0.125	0.41	4.91	0.43	8.03
CHA NC	0.082	0.209	0.071	0.166	0.39	4.78	0.43	6.02
CHI IL	0.125	0.267	0.090	0.168	0.47	3.74	0.54	5.95
CIN OH	0.070	0.191	0.046	0.123	0.37	5.24	0.38	8.16
CLE OH	0.057	0.147	0.035	0.088	0.39	6.82	0.40	11.33
DAL TX	0.040	0.115	0.033	0.091	0.35	8.66	0.36	10.95
DEN CO	0.044	0.107	0.030	0.073	0.41	9.32	0.41	13.70
DET MI	0.074	0.198	0.048	0.127	0.37	5.05	0.38	7.88
ELP TX	0.043	0.113	0.032	0.079	0.38	8.86	0.41	12.69
HAR CT	0.077	0.206	0.059	0.145	0.37	4.85	0.41	6.88
HOU TX	0.073	0.186	0.045	0.112	0.39	5.37	0.41	8.96
IND IN	0.059	0.156	0.041	0.105	0.38	6.40	0.39	9.51
JAC FL	0.072	0.165	0.066	0.143	0.44	6.07	0.46	6.99
KAN MO	0.071	0.197	0.054	0.142	0.36	5.07	0.38	7.07
LAK LA	0.111	0.224	0.075	0.134	0.50	4.47	0.56	7.49
LOS CA	0.067	0.150	0.038	0.084	0.45	6.69	0.45	11.90
LOU KY	0.073	0.187	0.054	0.132	0.39	5.34	0.41	7.56
MEM TN	0.083	0.205	0.057	0.133	0.41	4.89	0.43	7.54
MIA FL	0.076	0.182	0.074	0.173	0.42	5.49	0.43	5.80
NAS TN	0.091	0.236	0.078	0.193	0.39	4.23	0.40	5.19
NEW NY	0.106	0.174	0.052	0.089	0.61	5.75	0.58	11.21
PHI PA	0.065	0.168	0.044	0.110	0.39	5.95	0.40	9.07
PHO AZ	0.055	0.161	0.034	0.094	0.34	6.20	0.36	10.63
POR OR	0.067	0.176	0.058	0.141	0.38	5.68	0.41	7.08
RIC VA	0.069	0.186	0.045	0.115	0.37	5.39	0.39	8.73
SAC CA	0.061	0.170	0.043	0.118	0.36	5.88	0.37	8.48
SAI MO	0.054	0.141	0.032	0.081	0.39	7.10	0.39	12.28
SAL UT	0.068	0.188	0.045	0.116	0.36	5.33	0.39	8.61
SAN TX	0.043	0.126	0.040	0.116	0.34	7.95	0.35	8.64
SDO CA	0.051	0.117	0.041	0.091	0.44	8.53	0.45	11.00
SFO CA	0.018	0.055	0.017	0.050	0.33	18.20	0.34	20.01
TAM FL	0.053	0.133	0.037	0.091	0.40	7.52	0.41	10.99
TUL OK	0.071	0.178	0.044	0.111	0.40	5.61	0.40	9.03
WAS DC	0.075	0.194	0.044	0.112	0.39	5.14	0.40	8.96

CONCLUSIONS

The decision whether it is appropriate to regulate a compound as an ozone precursor requires a qualitative assessment of its ozone impacts under a variety of environmental conditions. This involves developing a chemical mechanism for the compounds atmospheric reactions which can be reliably used in airshed models to predict its atmospheric reactivity. Until this study, there was no information concerning the atmospheric reactions of methyl acetate, and thus reactivity estimates for this compound were highly uncertain. The objective of this study was to provide the data needed to verify the predictive capabilities of an reaction mechanism for methyl acetate, and thus allow for more reliable estimates of its atmospheric ozone impacts. We believe this program addressed this objective.

Prior to this study, atmospheric reactivity estimates for methyl acetate were based on a mechanism involving the overall formation of two molecules of formaldehyde and two NO to NO₂ conversions and the regeneration of OH radicals. This is based on an assumed rapid β -scission decomposition of the $\cdot\text{CH}_2\text{O}(\text{CO})\text{CH}_3$ radical to $\text{HCHO} + \text{CO}_2 + \text{CH}_3\cdot$. This study has shown that this mechanism is incorrect, since contrary to its predictions the addition of methyl acetate did not significantly increase formaldehyde formation, and the effect of methyl acetate on NO oxidation and O₃ formation was found to be significantly less than predicted by this mechanism. On the other hand, the data obtained are well predicted by an alternative mechanism which assumes that the $\cdot\text{CH}_2\text{O}(\text{CO})\text{CH}_3$ radical decomposes only slowly if at all, but instead reacts primarily with O₂, forming $\text{H}(\text{CO})\text{O}(\text{CO})\text{OCH}_3$ as the major methyl acetate oxidation product. Note that the analytical techniques available at our laboratory were not sufficient to monitor this compound, and separate product studies, probably using in-situ FT-IR spectroscopy, would be necessary to confirm our prediction that this indeed is the major product formed. However, the good performance of this mechanism in simulating the chamber data, using two different base ROG mixtures and two different NO_x conditions, gives us reason to believe that this mechanism should give reasonably reliable predictions of methyl acetate's reactivity under atmospheric conditions.

If this experimentally-verified modified methyl acetate mechanism is assumed, the atmospheric ozone impact of methyl acetate is calculated to be approximately 1/3 to 1/2 that of ethane, on an ozone formed per gram VOC basis. There is relatively little scenario-to-scenario variability in the methyl acetate / ethane reactivity ratio, and there was no scenario we examined where methyl acetate was found to have a greater ozone impact as ethane. Similar results are obtained regardless of whether ozone impacts are quantified by peak ozone yields or integrated ozone over the standard, nor were the results found to be highly dependent on NO_x conditions. Therefore, we conclude that methyl acetate can be considered to have a lower ozone reactivity than ethane under most, if not all, atmospheric conditions of relevance to the assessment of ozone control strategies.

REFERENCES

- Atkinson, R. (1987): "A Structure-Activity Relationship for the Estimation of Rate Constants for the Gas-Phase Reactions of OH Radicals with Organic Compounds," *Int. J. Chem. Kinet.*, 19, 799-828.
- Atkinson, R. (1989): "Kinetics and Mechanisms of the Gas-Phase Reactions of the Hydroxyl Radical with Organic Compounds," *J. Phys. Chem. Ref. Data*, Monograph no 1.
- Atkinson, R. (1991): "Kinetics and Mechanisms of the Gas-Phase Reactions of the NO₃ Radical with Organic Compounds," *J. Phys. Chem. Ref. Data*, 20, 459-507.
- Atkinson, R. and W. P. L. Carter (1984): "Kinetics and Mechanisms of the Gas-Phase Reactions of Ozone with Organic Compounds under Atmospheric Conditions," *Chem. Rev.* 1984, 437-470.
- Baugues, K. (1990): "Preliminary Planning Information for Updating the Ozone Regulatory Impact Analysis Version of EKMA," Draft Document, Source Receptor Analysis Branch, Technical Support Division, U. S. Environmental Protection Agency, Research Triangle Park, NC, January.
- Campbell, I. M. and P. E. Parkinson (1978): *Chem. Phys. Lett.* 53, 385.
- CARB (1993): "Proposed Regulations for Low-Emission Vehicles and Clean Fuels — Staff Report and Technical Support Document," California Air Resources Board, Sacramento, CA, August 13, 1990. See also Appendix VIII of "California Exhaust Emission Standards and Test Procedures for 1988 and Subsequent Model Passenger Cars, Light Duty Trucks and Medium Duty Vehicles," as last amended September 22, 1993. Incorporated by reference in Section 1960.1 (k) of Title 13, California Code of Regulations.
- Calvert, J. G., and J. N. Pitts, Jr. (1966): *Photochemistry*, John Wiley and Sons, New York.
- Carter, W. P. L. (1990): "A Detailed Mechanism for the Gas-Phase Atmospheric Reactions of Organic Compounds," *Atmos. Environ.*, 24A, 481-518.
- Carter, W. P. L. (1991): "Development of Ozone Reactivity Scales for Volatile Organic Compounds", EPA-600/3-91/050, August.
- Carter, W. P. L. (1993): "Development and Application of an Up-To-Date Photochemical Mechanism for Airshed Modeling and Reactivity Assessment," Draft final report for California Air Resources Board Contract No. A934-094, April 26.
- Carter, W. P. L. (1994a): "Development of Ozone Reactivity Scales for Volatile Organic Compounds," *J. Air & Waste Manage. Assoc.*, 44, 881-899.
- Carter, W. P. L. (1994b): "Calculation of Reactivity Scales Using an Updated Carbon Bond IV Mechanism," Draft Report Prepared for Systems Applications International Under Funding from the Auto/Oil Air Quality Improvement Research Program, April 12.

- Carter, W. P. L. (1995): "Computer Modeling of Environmental Chamber Measurements of Maximum Incremental Reactivities of Volatile Organic Compounds," *Atmos. Environ.*, 29, 2513-2517.
- Carter, W. P. L. and R. Atkinson (1987): "An Experimental Study of Incremental Hydrocarbon Reactivity," *Environ. Sci. Technol.*, 21, 670-679
- Carter, W. P. L. and R. Atkinson (1989a): "A Computer Modeling Study of Incremental Hydrocarbon Reactivity", *Environ. Sci. Technol.*, 23, 864.
- Carter, W. P. L. and R. Atkinson (1989b): "Alkyl Nitrate Formation from the Atmospheric Photooxidation of Alkanes; a Revised Estimation Method," *J. Atm. Chem.* 8, 165-173.
- Carter, W. P. L., and F. W. Lurmann (1990): "Evaluation of the RADM Gas-Phase Chemical Mechanism," Final Report, EPA-600/3-90-001.
- Carter, W. P. L. and F. W. Lurmann (1991): "Evaluation of a Detailed Gas-Phase Atmospheric Reaction Mechanism using Environmental Chamber Data," *Atm. Environ.* 25A, 2771-2806.
- Carter, W. P. L., D. Luo, I. L. Malkina, and J. A. Pierce (1993a): "An Experimental and Modeling Study of the Photochemical Ozone Reactivity of Acetone," Final Report to Chemical Manufacturers Association Contract No. KET-ACE-CRC-2.0. December 10.
- Carter, W. P. L., J. A. Pierce, I. L. Malkina, D. Luo and W. D. Long (1993b): "Environmental Chamber Studies of Maximum Incremental Reactivities of Volatile Organic Compounds," Report to Coordinating Research Council, Project No. ME-9, California Air Resources Board Contract No. A032-0692; South Coast Air Quality Management District Contract No. C91323, United States Environmental Protection Agency Cooperative Agreement No. CR-814396-01-0, University Corporation for Atmospheric Research Contract No. 59166, and Dow Corning Corporation. April 1.
- Carter, W. P. L., D. Luo, I. L. Malkina, and J. A. Pierce (1995a): "Environmental Chamber Studies of Atmospheric Reactivities of Volatile Organic Compounds. Effects of Varying ROG Surrogate and NO_x," Final report to Coordinating Research Council, Inc., Project ME-9, California Air Resources Board, Contract A032-0692, and South Coast Air Quality Management District, Contract C91323. March 24.
- Carter, W. P. L., D. Luo, I. L. Malkina, and D. Fitz (1995b): "The University of California, Riverside Environmental Chamber Data Base for Evaluating Oxidant Mechanism. Indoor Chamber Experiments through 1993," Report submitted to the U. S. Environmental Protection Agency, EPA/AREAL, Research Triangle Park, NC., March 20..
- Carter, W. P. L., J. A. Pierce, D. Luo, and I. L. Malkina (1995c): "Environmental Chamber Study of Maximum Incremental Reactivities of Volatile Organic Compounds," *Atmos. Environ.* 29, 2499-2511.

- Carter, W. P. L., D. Luo, I. L. Malkina, and J. A. Pierce (1995d): "Environmental Chamber Studies of Atmospheric Reactivities of Volatile Organic Compounds. Effects of Varying Chamber and Light Source," Final report to National Renewable Energy Laboratory, Contract XZ-2-12075, Coordinating Research Council, Inc., Project M-9, California Air Resources Board, Contract A032-0692, and South Coast Air Quality Management District, Contract C91323, March 26.
- Chang, T. Y. and S. J. Rudy (1990): "Ozone-Forming Potential of Organic Emissions from Alternative-Fueled Vehicles," *Atmos. Environ.*, 24A, 2421-2430.
- Croes, B. E., Technical Support Division, California Air Resources Board, personal communication (1991).
- Croes, B. E., et al. (1994): "Southern California Air Quality Study Data Archive," Research Division, California Air Resources Board.
- Dodge, M. C. (1984): "Combined effects of organic reactivity and NMHC/NO_x ratio on photochemical oxidant formation -- a modeling study," *Atmos. Environ.*, 18, 1657.
- EPA (1984): "Guideline for Using the Carbon Bond Mechanism in City-Specific EKMA," EPA-450/4-84-005, February.
- Gery, M. W., R. D. Edmond and G. Z. Whitten (1987): "Tropospheric Ultraviolet Radiation. Assessment of Existing Data and Effects on Ozone Formation," Final Report, EPA-600/3-87-047, October.
- Gipson, G. L., W. P. Freas, R. A. Kelly and E. L. Meyer, "Guideline for Use of City-Specific EKMA in Preparing Ozone SIPs, EPA-450/4-80-027, March, 1981.
- Gipson, G. L. and W. P. Freas (1983): "Use of City-Specific EKMA in the Ozone RIA," U. S. Environmental Protection Agency, July.
- Gipson, G. L. (1984): "Users Manual for OZIPM-2: Ozone Isopleth Plotting Package With Optional Mechanism/Version 2," EPA-450/4-84-024, August.
- Hogo, H. and M. W. Gery (1988): "Guidelines for Using OZIPM-4 with CBM-IV or Optional Mechanisms. Volume 1. Description of the Ozone Isopleth Plotting Package Version 4", Final Report for EPA Contract No. 68-02-4136, Atmospheric Sciences Research Laboratory, Research Triangle Park, NC. January.
- Jeffries, H. E., K. G. Sexton, J. R. Arnold, and T. L. Kale (1989): "Validation Testing of New Mechanisms with Outdoor Chamber Data. Volume 2: Analysis of VOC Data for the CB4 and CAL Photochemical Mechanisms," Final Report, EPA-600/3-89-010b.
- Jeffries, H. E. and R. Crouse (1991): "Scientific and Technical Issues Related to the Application of Incremental Reactivity. Part II: Explaining Mechanism Differences," Report prepared for Western States Petroleum Association, Glendale, CA, October.
- Jeffries, H. E. (1991): "UNC Solar Radiation Models," unpublished draft report for EPA Cooperative Agreements CR813107, CR813964 and CR815779". Undated.

- Johnson, G. M. (1983): "Factors Affecting Oxidant Formation in Sydney Air," in "The Urban Atmosphere -- Sydney, a Case Study." Eds. J. N. Carras and G. M. Johnson (CSIRO, Melbourne), pp. 393-408.
- Lurmann, F. W. and H. H. Main (1992): "Analysis of the Ambient VOC Data Collected in the Southern California Air Quality Study," Final Report to California Air Resources Board Contract No. A832-130, February.
- Pitts, J. N., Jr., E. Sanhueza, R. Atkinson, W. P. L. Carter, A. M. Winer, G. W. Harris, and C. N. Plum (1984): "An Investigation of the Dark Formation of Nitrous Acid in Environmental Chambers," *Int. J. Chem. Kinet.*, 16, 919-939.
- Tuazon, E. C., R. Atkinson, C. N. Plum, A. M. Winer, and J. N. Pitts, Jr. (1983): "The Reaction of Gas-Phase N_2O_5 with Water Vapor," *Geophys. Res. Lett.* 10, 953-956.
- Wallington, T. J., P. Dagaut, R. Liu, and M. J. Kurylo (1988): *Int. J. Chem. Kinet.* 20, 177.
- Zafonte, L., P. L. Rieger, and J. R. Holmes (1977): "Nitrogen Dioxide Photolysis in the Los Angeles Atmosphere," *Environ. Sci. Technol.* 11, 483-487.

APPENDIX A
LISTING OF THE CHEMICAL MECHANISM

The chemical mechanism used in the environmental chamber and atmospheric model simulations discussed in this report is given in Tables A-1 through A-4. Table A-1 lists the species used in the mechanism, Table A-2 gives the reactions and rate constants, Table A-3 gives the parameters used to calculate the rates of the photolysis reactions, and Table A-4 gives the values and derivations of the chamber-dependent parameters used when modeling the environmental chamber experiments. Footnotes to Table A-2 indicate the format used for the reaction listing.

Table A-1. List of species in the chemical mechanism used in the model simulations for this study.

Name	Description
Constant Species.	
O2	Oxygen
M	Air
H2O	Water
Active Inorganic Species.	
O3	Ozone
NO	Nitric Oxide
NO2	Nitrogen Dioxide
NO3	Nitrate Radical
N2O5	Nitrogen Pentoxide
HONO	Nitrous Acid
HNO3	Nitric Acid
HNO4	Peroxynitric Acid
HO2H	Hydrogen Peroxide
Active Radical Species and Operators.	
HO2.	Hydroperoxide Radicals
RO2.	Operator to Calculate Total Organic Peroxy Radicals
RCO3.	Operator to Calculate Total Acetyl Peroxy Radicals
Active Reactive Organic Product Species.	
CO	Carbon Monoxide
HCHO	Formaldehyde
CCHO	Acetaldehyde
RCHO	Lumped C3+ Aldehydes
ACET	Acetone

Table A-1, (continued)

Name	Description
MEK	Lumped Ketones
PHEN	Phenol
CRES	Cresols
BALD	Aromatic aldehydes (e.g., benzaldehyde)
GLY	Glyoxal
MGLY	Methyl Glyoxal
AFG1	Reactive Aromatic Fragmentation Products from benzene and naphthalene
AFG2	Other Reactive Aromatic Fragmentation Products
AFG3	Aromatic Fragmentation Products used in adjusted m-xylene mechanism
RNO3	Organic Nitrates
NPHE	Nitrophenols
ISOPROD	Lumped isoprene product species
PAN	Peroxy Acetyl Nitrate
PPN	Peroxy Propionyl Nitrate
GPAN	PAN Analogue formed from Glyoxal
PBZN	PAN Analogues formed from Aromatic Aldehydes
-OOH	Operator Representing Hydroperoxy Groups

Non-Reacting Species

CO2	Carbon Dioxide
-C	"Lost Carbon"
-N	"Lost Nitrogen"
H2	Hydrogen

Steady State Species and Operators.

HO.	Hydroxyl Radicals
O	Ground State Oxygen Atoms
O*1D2	Excited Oxygen Atoms
RO2-R.	Peroxy Radical Operator representing NO to NO ₂ conversion with HO ₂ formation.
RO2-N.	Peroxy Radical Operator representing NO consumption with organic nitrate formation.
RO2-NP.	Peroxy Radical Operator representing NO consumption with nitrophenol formation
R2O2.	Peroxy Radical Operator representing NO to NO ₂ conversion.
CCO-O2.	Peroxy Acetyl Radicals
C2CO-O2.	Peroxy Propionyl Radicals
HCOCO-O2.	Peroxyacyl Radical formed from Glyoxal
BZ-CO-O2.	Peroxyacyl Radical formed from Aromatic Aldehydes
HOCOO.	Intermediate formed in Formaldehyde + HO ₂ reaction
BZ-O.	Phenoxy Radicals
BZ(NO2)-O.	Nitratophenoxy Radicals
HOCOO.	Radical Intermediate formed in the HO ₂ + Formaldehyde system.
(HCHO2)	Excited Criegee biradicals formed from =CH ₂ groups
(CCHO2)	Excited Criegee biradicals formed from =CHCH ₃ groups
(RCHO2)	Excited Criegee biradicals formed from =CHR groups, where R not CH ₃
(C(C)CO2)	Excited Criegee biradicals formed from =C(CH ₃) ₂ groups

Table A-1, (continued)

Name	Description
(C(R)CO2)	Excited Criegee biradicals formed from =C(CH ₃)R or CR ₂ groups
(BZCHO2)	Excited Criegee biradicals formed from styrenes

Hydrocarbon species represented explicitly

CH4	Methane (EKMA simulations only)
ETHANE	Ethane (Ethane reactivity simulations only)
N-C4	n-Butane (Chamber simulations only)
N-C6	n-Hexane (Chamber simulations only)
N-C8	n-Octane (Chamber simulations only)
ETHE	Ethene
ISOP	Isoprene (EKMA Simulations only)
APIN	α-Pinene (EKMA Simulations only)
UNKN	Unknown biogenics. (EKMA Simulations only)
PROPENE	Propene (Chamber simulations only)
T-2-BUTE	<u>trans</u> -2-Butene (Chamber simulations only)
TOLUENE	Toluene (Chamber simulations only)
M-XYLENE	m-Xylene (Chamber simulations only)
ME-ACET	Methyl Acetate

Lumped species used to represent the Base ROG mixture in the EKMA model simulations.

ALK1	Alkanes and other saturated compounds with $k_{OH} < 10^4 \text{ ppm}^{-1} \text{ min}^{-1}$.
ALK2	Alkanes and other saturated compounds with $k_{OH} \geq 10^4 \text{ ppm}^{-1} \text{ min}^{-1}$.
ARO1	Aromatics with $k_{OH} < 2 \times 10^4 \text{ ppm}^{-1} \text{ min}^{-1}$.
ARO2	Aromatics with $k_{OH} \geq 2 \times 10^4 \text{ ppm}^{-1} \text{ min}^{-1}$.
OLE2	Alkenes (other than ethene) with $k_{OH} < 7 \times 10^4 \text{ ppm}^{-1} \text{ min}^{-1}$.
OLE3	Alkenes with $k_{OH} \geq 7 \times 10^4 \text{ ppm}^{-1} \text{ min}^{-1}$.

Table A-2. List of reactions in the chemical mechanism used in the model simulations for this study.

Rxn.	Kinetic Parameters [a]				Reactions [b]
Label	k(300)	A	Ea	B	
Inorganic Reactions					
1	(Phot. Set = NO2)				NO2 + HV = NO + O
2	6.00E-34	6.00E-34	0.00	-2.30	O + O2 + M = O3 + M
3A	9.69E-12	6.50E-12	-0.24	0.00	O + NO2 = NO + O2
3B	1.55E-12	(Falloff Kinetics)			O + NO2 = NO3 + M
	k0 =	9.00E-32	0.00	-2.00	
	kINF =	2.20E-11	0.00	0.00	
	F=	0.60	n=	1.00	
4	1.88E-14	2.00E-12	2.78	0.00	O3 + NO = NO2 + O2
5	3.36E-17	1.40E-13	4.97	0.00	O3 + NO2 = O2 + NO3
6	2.80E-11	1.70E-11	-0.30	0.00	NO + NO3 = 2 NO2
7	1.92E-38	3.30E-39	-1.05	0.00	NO + NO + O2 = 2 NO2
8	1.26E-12	(Falloff Kinetics)			NO2 + NO3 = N2O5
	k0 =	2.20E-30	0.00	-4.30	
	kINF =	1.50E-12	0.00	-0.50	
	F=	0.60	n=	1.00	
9	5.53E+10	9.09E+26	22.26	0.00	N2O5 + #RCO8 = NO2 + NO3
10	1.00E-21	(No T Dependence)			N2O5 + H2O = 2 HNO3
11	4.17E-16	2.50E-14	2.44	0.00	NO2 + NO3 = NO + NO2 + O2
12A	(Phot. Set = NO3NO)				NO3 + HV = NO + O2
12B	(Phot. Set = NO3NO2)				NO3 + HV = NO2 + O
13A	(Phot. Set = O3O3P)				O3 + HV = O + O2
13B	(Phot. Set = O3O1D)				O3 + HV = O*1D2 + O2
14	2.20E-10	(No T Dependence)			O*1D2 + H2O = 2 HO.
15	2.92E-11	1.92E-11	-0.25	0.00	O*1D2 + M = O + M
16	4.81E-12	(Falloff Kinetics)			HO. + NO = HONO
	k0 =	7.00E-31	0.00	-2.60	
	kINF =	1.50E-11	0.00	-0.50	
	F=	0.60	n=	1.00	
17	(Phot. Set = HONO)				HONO + HV = HO. + NO
18	1.13E-11	(Falloff Kinetics)			HO. + NO2 = HNO3
	k0 =	2.60E-30	0.00	-3.20	
	kINF =	2.40E-11	0.00	-1.30	
	F=	0.60	n=	1.00	
19	1.03E-13	6.45E-15	-1.65	0.00	HO. + HNO3 = H2O + NO3
21	2.40E-13	(No T Dependence)			HO. + CO = HO2. + CO2
22	6.95E-14	1.60E-12	1.87	0.00	HO. + O3 = HO2. + O2
23	8.28E-12	3.70E-12	-0.48	0.00	HO2. + NO = HO. + NO2
24	1.37E-12	(Falloff Kinetics)			HO2. + NO2 = HNO4
	k0 =	1.80E-31	0.00	-3.20	
	kINF =	4.70E-12	0.00	-1.40	
	F=	0.60	n=	1.00	
25	7.92E+10	4.76E+26	21.66	0.00	HNO4 + #RCO24 = HO2. + NO2
27	4.61E-12	1.30E-12	-0.75	0.00	HNO4 + HO. = H2O + NO2 + O2
28	2.08E-15	1.10E-14	0.99	0.00	HO2. + O3 = HO. + 2 O2
29A	1.73E-12	2.20E-13	-1.23	0.00	HO2. + HO2. = HO2H + O2
29B	5.00E-32	1.90E-33	-1.95	0.00	HO2. + HO2. + M = HO2H + O2
29C	3.72E-30	3.10E-34	-5.60	0.00	HO2. + HO2. + H2O = HO2H + O2 + H2O
29D	2.65E-30	6.60E-35	-6.32	0.00	HO2. + HO2. + H2O = HO2H + O2 + H2O
30A	1.73E-12	2.20E-13	-1.23	0.00	NO3 + HO2. = HNO3 + O2
30B	5.00E-32	1.90E-33	-1.95	0.00	NO3 + HO2. + M = HNO3 + O2
30C	3.72E-30	3.10E-34	-5.60	0.00	NO3 + HO2. + H2O = HNO3 + O2 + H2O
30D	2.65E-30	6.60E-35	-6.32	0.00	NO3 + HO2. + H2O = HNO3 + O2 + H2O
31	(Phot. Set = H2O2)				HO2H + HV = 2 HO.
32	1.70E-12	3.30E-12	0.40	0.00	HO2H + HO. = HO2. + H2O
33	9.90E-11	4.60E-11	-0.46	0.00	HO. + HO2. = H2O + O2
Peroxy Radical Operators					
B1	7.68E-12	4.20E-12	-0.36	0.00	RO2. + NO = NO
B2	2.25E-11	(Falloff Kinetics)			RCO3. + NO = NO
	k0 =	5.65E-28	0.00	-7.10	
	kINF =	2.64E-11	0.00	-0.90	
	F=	0.27	n=	1.00	
B4	1.04E-11	(Falloff Kinetics)			RCO3. + NO2 = NO2
	k0 =	2.57E-28	0.00	-7.10	
	kINF =	1.20E-11	0.00	-0.90	
	F=	0.30	n=	1.00	
B5	4.90E-12	3.40E-13	-1.59	0.00	RO2. + HO2. = HO2. + RO2-HO2-PROD
B6	4.90E-12	3.40E-13	-1.59	0.00	RCO3. + HO2. = HO2. + RO2-HO2-PROD
B8	1.00E-15	(No T Dependence)			RO2. + RO2. = RO2-RO2-PROD
B9	1.09E-11	1.86E-12	-1.05	0.00	RO2. + RCO3. = RO2-RO2-PROD
B10	1.64E-11	2.80E-12	-1.05	0.00	RCO3. + RCO3. = RO2-RO2-PROD

Table A-2 (continued)

Rxn.	Kinetic Parameters [a]				Reactions [b]
Label	k(300)	A	Ea	B	
B11	(Same k as for RO2.)			RO2-R. + NO = NO2 + HO2.
B12	(Same k as for RO2.)			RO2-R. + HO2. = -OOH
B13	(Same k as for RO2.)			RO2-R. + RO2. = RO2. + 0.5 HO2.
B14	(Same k as for RO2.)			RO2-R. + RCO3. = RCO3. + 0.5 HO2.
B19	(Same k as for RO2.)			RO2-N. + NO = RNO3
B20	(Same k as for RO2.)			RO2-N. + HO2. = -OOH + MEK + 1.5 -C
B21	(Same k as for RO2.)			RO2-N. + RO2. = RO2. + 0.5 HO2. + MEK + 1.5 -C
B22	(Same k as for RO2.)			RO2-N. + RCO3. = RCO3. + 0.5 HO2. + MEK + 1.5 -C
B15	(Same k as for RO2.)			R2O2. + NO = NO2
B16	(Same k as for RO2.)			R2O2. + HO2. =
B17	(Same k as for RO2.)			R2O2. + RO2. = RO2.
B18	(Same k as for RO2.)			R2O2. + RCO3. = RCO3.
B23	(Same k as for RO2.)			RO2-XN. + NO = -N
B24	(Same k as for RO2.)			RO2-XN. + HO2. = -OOH
B25	(Same k as for RO2.)			RO2-XN. + RO2. = RO2. + 0.5 HO2.
B26	(Same k as for RO2.)			RO2-XN. + RCO3. = RCO3. + HO2.
G2	(Same k as for RO2.)			RO2-NP. + NO = NPHE
G3	(Same k as for RO2.)			RO2-NP. + HO2. = -OOH + 6 -C
G4	(Same k as for RO2.)			RO2-NP. + RO2. = RO2. + 0.5 HO2. + 6 -C
G5	(Same k as for RO2.)			RO2-NP. + RCO3. = RCO3. + HO2. + 6 -C
Excited Criegee Biradicals					
RZ1	(fast)				(HCHO2) = 0.7 HCOOH + 0.12 "HO. + HO2. + CO" + 0.18 "H2 + CO2"
RZ2	(fast)				(CCHO2) = 0.25 CCOOH + 0.15 "CH4 + CO2" + 0.6 HO. + 0.3 "CCO-O2. + RCO3." + 0.3 "RO2-R. + HCHO + CO + RO2."
RZ3	(fast)				(RCHO2) = 0.25 CCOOH + 0.15 CO2 + 0.6 HO. + 0.3 "C2CO-O2. + RCO3." + 0.3 "RO2-R. + CCHO + CO + RO2." + 0.55 -C
RZ4	(fast)				(C(C)CO2) = HO. + R2O2. + HCHO + CCO-O2. + RCO3. + RO2.
RZ5	(fast)				(C(R)CO2) = HO. + CCO-O2. + CCHO + R2O2. + RCO3. + RO2.
RZ6	(fast)				(CYCCO2) = 0.3 "HO. + C2CO-O2. + R2O2. + RCO3. + RO2." + 0.3 RCHO + 4.2 -C
RZ8	(fast)				(BZCHO2) = 0.5 "BZ-O. + R2O2. + CO + HO."
ISZ1	(fast)				(C:CC(C)O2) = HO. + R2O2. + HCHO + C2CO-O2. + RO2. + RCO3.
ISZ2	(fast)				(C:C(C)CHO2) = 0.75 RCHO + 0.25 ISOPROD + 0.5 -C
MAZ1	(fast)				(C2(O2)CHO) = HO. + R2O2. + HCHO + HCOCO-O2. + RO2. + RCO3.
MLZ1	(fast)				(HOCCHO2) = 0.6 HO. + 0.3 "CCO-O2. + RCO3." + 0.3 "RO2-R. + HCHO + CO + RO2." + 0.8 -C
MZ1	(fast)				(HCOCHO2) = 0.12 "HO2. + 2 CO + HO." + 0.74 -C + 0.51 "CO2 + HCHO"
MZ2	(fast)				(C2(O2)COH) = HO. + MGLY + HO2. + R2O2. + RO2.
Organic Product Species					
B7	(Phot. Set = CO2H)			-OOH + HV = HO2. + HO.
B7A	1.81E-12	1.18E-12	-0.25	0.00	HO. + -OOH = HO.
B7B	3.71E-12	1.79E-12	-0.44	0.00	HO. + -OOH = RO2-R. + RO2.
C1	(Phot. Set = HCHONEWR)				HCHO + HV = 2 HO2. + CO
C2	(Phot. Set = HCHONEWM)				HCHO + HV = H2 + CO
C3	9.76E-12	1.13E-12	-1.29	2.00	HCHO + HO. = HO2. + CO + H2O
C4	7.79E-14	9.70E-15	-1.24	0.00	HCHO + HO2. = HOCOO.
C4A	1.77E+02	2.40E+12	13.91	0.00	HOCOO. = HO2. + HCHO
C4B	(Same k as for RO2.)			HOCOO. + NO = -C + NO2 + HO2.
C9	6.38E-16	2.80E-12	5.00	0.00	HCHO + NO3 = HNO3 + HO2. + CO
C10	1.57E-11	5.55E-12	-0.62	0.00	CCHO + HO. = CCO-O2. + H2O + RCO3.
C11A	(Phot. Set = CCHOR)			CCHO + HV = CO + HO2. + HCHO + RO2-R. + RO2.
C12	2.84E-15	1.40E-12	3.70	0.00	CCHO + NO3 = HNO3 + CCO-O2. + RCO3.
C25	1.97E-11	8.50E-12	-0.50	0.00	RCHO + HO. = C2CO-O2. + RCO3.
C26	(Phot. Set = RCHO)			RCHO + HV = CCHO + RO2-R. + RO2. + CO + HO2.
C27	2.84E-15	1.40E-12	3.70	0.00	NO3 + RCHO = HNO3 + C2CO-O2. + RCO3.
C38	2.23E-13	4.81E-13	0.46	2.00	ACET + HO. = R2O2. + HCHO + CCO-O2. + RCO3. + RO2.
C39	(Phot. Set = ACET-93C)				ACET + HV = CCO-O2. + HCHO + RO2-R. + RCO3. + RO2.
C44	1.16E-12	2.92E-13	-0.82	2.00	MEK + HO. = H2O + 0.5 "CCHO + HCHO + CCO-O2. + C2CO-O2." + RCO3. + 1.5 "R2O2. + RO2."
C57	(Phot. Set = KETONE)			MEK + HV + #0.1 = CCO-O2. + CCHO + RO2-R. + RCO3. + RO2.

Table A-2 (continued)

Rxn. Label	Kinetic Parameters [a]				Reactions [b]
	k(300)	A	Ea	B	
C95	2.07E-12	2.19E-11	1.41	0.00	RNO3 + HO. = NO2 + 0.155 MEK + 1.05 RCHO + 0.48 CCHO + 0.16 HCHO + 0.11 -C + 1.39 "R2O2. + RO2."
C58A		(Phot. Set = GLYOXAL1)			GLY + HV = 0.8 HO2. + 0.45 HCHO + 1.55 CO
C58B		(Phot. Set = GLYOXAL2)			GLY + HV + #0.029 = 0.13 HCHO + 1.87 CO
C59	1.14E-11	(No T Dependence)			GLY + HO. = 0.6 HO2. + 1.2 CO + 0.4 "HCOCO-O2. + RCO3."
C60		(Same k as for CCHO)			GLY + NO3 = HNO3 + 0.6 HO2. + 1.2 CO + 0.4 "HCOCO-O2. + RCO3."
C68A		(Phot. Set = MEGLYOX1)			MGLY + HV = HO2. + CO + CCO-O2. + RCO3.
C68B		(Phot. Set = MEGLYOX2)			MGLY + HV + 0.107 = HO2. + CO + CCO-O2. + RCO3.
C69	1.72E-11	(No T Dependence)			MGLY + HO. = CO + CCO-O2. + RCO3.
C70		(Same k as for CCHO)			MGLY + NO3 = HNO3 + CO + CCO-O2. + RCO3.
G7	1.14E-11	(No T Dependence)			HO. + AFG1 = HCOCO-O2. + RCO3.
G8		(Phot. Set = ACROLEIN)			AFG1 + HV + #0.029 = HO2. + HCOCO-O2. + RCO3.
U2OH	1.72E-11	(No T Dependence)			HO. + AFG2 = C2CO-O2. + RCO3.
U2HV		(Phot. Set = ACROLEIN)			AFG2 + HV = HO2. + CO + CCO-O2. + RCO3.
G46	2.63E-11	(No T Dependence)			HO. + PHEN = 0.15 RO2-NP. + 0.85 RO2-R. + 0.2 GLY + 4.7 -C + RO2.
G51	3.60E-12	(No T Dependence)			NO3 + PHEN = HNO3 + BZ-O.
G52	4.20E-11	(No T Dependence)			HO. + CRES = 0.15 RO2-NP. + 0.85 RO2-R. + 0.2 MGLY + 5.5 -C + RO2.
G57	2.10E-11	(No T Dependence)			NO3 + CRES = HNO3 + BZ-O. + -C
G30	1.29E-11	(No T Dependence)			BALD + HO. = BZ-CO-O2. + RCO3.
G31		(Phot. Set = BZCHO)			BALD + HV + #0.05 = 7 -C
G32	2.61E-15	1.40E-12	3.75	0.00	BALD + NO3 = HNO3 + BZ-CO-O2.
G58	3.60E-12	(No T Dependence)			NPHE + NO3 = HNO3 + BZ(NO2)-O.
G59		(Same k as for BZ-O.)			BZ(NO2)-O. + NO2 = 2 -N + 6 -C
G60		(Same k as for RO2.)			BZ(NO2)-O. + HO2. = NPHE
G61		(Same k as for BZ-O.)			BZ(NO2)-O. = NPHE
C13		(Same k as for RCO3.)			CCO-O2. + NO = CO2 + NO2 + HCHO + RO2-R. + RO2.
C14		(Same k as for RCO3.)			CCO-O2. + NO2 = PAN
C15		(Same k as for RCO3.)			CCO-O2. + HO2. = -OOH + CO2 + HCHO
C16		(Same k as for RCO3.)			CCO-O2. + RO2. = RO2. + 0.5 HO2. + CO2 + HCHO
C17		(Same k as for RCO3.)			CCO-O2. + RCO3. = RCO3. + HO2. + CO2 + HCHO
C18	6.50E-04	(Falloff Kinetics)			PAN = CCO-O2. + NO2 + RCO3.
	k0 =	4.90E-03	23.97	0.00	
	kINF =	4.00E+16	27.08	0.00	
		F= 0.30	n= 1.00		
C28		(Same k as for RCO3.)			C2CO-O2. + NO = CCHO + RO2-R. + CO2 + NO2 + RO2.
C29	8.40E-12	(No T Dependence)			C2CO-O2. + NO2 = PPN
C30		(Same k as for RCO3.)			C2CO-O2. + HO2. = -OOH + CCHO + CO2
C31		(Same k as for RCO3.)			C2CO-O2. + RO2. = RO2. + 0.5 HO2. + CCHO + CO2
C32		(Same k as for RCO3.)			C2CO-O2. + RCO3. = RCO3. + HO2. + CCHO + CO2
C33	6.78E-04	1.60E+17	27.97	0.00	PPN = C2CO-O2. + NO2 + RCO3.
C62		(Same k as for RCO3.)			HCOCO-O2. + NO = NO2 + CO2 + CO + HO2.
C63		(Same k as for RCO3.)			HCOCO-O2. + NO2 = GPAN
C65		(Same k as for RCO3.)			HCOCO-O2. + HO2. = -OOH + CO2 + CO
C66		(Same k as for RCO3.)			HCOCO-O2. + RO2. = RO2. + 0.5 HO2. + CO2 + CO
C67		(Same k as for RCO3.)			HCOCO-O2. + RCO3. = RCO3. + HO2. + CO2 + CO
C64		(Same k as for PAN)			GPAN = HCOCO-O2. + NO2 + RCO3.
G33		(Same k as for RCO3.)			BZ-CO-O2. + NO = BZ-O. + CO2 + NO2 + R2O2. + RO2.
G43	3.53E-11	1.30E-11	-0.60	0.00	BZ-O. + NO2 = NPHE
G44		(Same k as for RO2.)			BZ-O. + HO2. = PHEN
G45	1.00E-03	(No T Dependence)			BZ-O. = PHEN
G34	8.40E-12	(No T Dependence)			BZ-CO-O2. + NO2 = PBZN
G36		(Same k as for RCO3.)			BZ-CO-O2. + HO2. = -OOH + CO2 + PHEN
G37		(Same k as for RCO3.)			BZ-CO-O2. + RO2. = RO2. + 0.5 HO2. + CO2 + PHEN
G38		(Same k as for RCO3.)			BZ-CO-O2. + RCO3. = RCO3. + HO2. + CO2 + PHEN
G35	2.17E-04	1.60E+15	25.90	0.00	PBZN = BZ-CO-O2. + NO2 + RCO3.
IPOH	3.36E-11	(No T Dependence)			ISOPROD + HO. = 0.293 CO + 0.252 CCHO + 0.126 HCHO + 0.041 GLY + 0.021 RCHO + 0.168 MGLY + 0.314 MEK + 0.503 RO2-R. + 0.21 CCO-O2. + 0.288 C2CO-O2. + 0.21 R2O2. + 0.713 RO2. + 0.498 RCO3. + -0.112 -C

Table A-2 (continued)

Rxn. Label	Kinetic Parameters [a]				Reactions [b]
	k(300)	A	Ea	B	
IPO3	7.11E-18	(No T Dependence)			ISOPROD + O3 = 0.02 CCHO + 0.04 HCHO + 0.01 GLY + 0.84 MGLY + 0.09 MEK + 0.66 (HCHO2) + 0.09 (HCOCHO2) + 0.18 (HOCCHO2) + 0.06 (C2(O2)CHO) + 0.01 (C2(O2)COH) + -0.39 -C
IPHV		(Phot. Set = ACROLEIN)			ISOPROD + HV + 0.0036 = 0.333 CO + 0.067 CCHO + 0.9 HCHO + 0.033 MEK + 0.333 HO2. + 0.7 RO2-R. + 0.267 CCO-O2. + 0.7 C2CO-O2. + 0.7 RO2. + 0.967 RCO3. + -0.133 -C
IPN3	1.00E-15	(No T Dependence)			ISOPROD + NO3 = 0.643 CO + 0.282 HCHO + 0.85 RNO3 + 0.357 RCHO + 0.925 HO2. + 0.075 C2CO-O2. + 0.075 R2O2. + 0.925 RO2. + 0.075 RCO3. + 0.075 HNO3 + -2.471 -C
Hydrocarbon Species Represented Explicitly					
	2.56E-12	1.36E-12	-0.38	2.00	N-C4 + HO. = 0.076 RO2-N. + 0.924 RO2-R. + 0.397 R2O2. + 0.001 HCHO + 0.571 CCHO + 0.14 RCHO + 0.533 MEK + -0.076 -C + 1.397 RO2.
	5.63E-12	1.35E-11	0.52	0.00	N-C6 + HO. = 0.185 RO2-N. + 0.815 RO2-R. + 0.738 R2O2. + 0.02 CCHO + 0.105 RCHO + 1.134 MEK + 0.186 -C + 1.738 RO2.
	8.76E-12	3.15E-11	0.76	0.00	N-C8 + HO. = 0.333 RO2-N. + 0.667 RO2-R. + 0.706 R2O2. + 0.002 RCHO + 1.333 MEK + 0.998 -C + 1.706 RO2.
	8.43E-12	1.96E-12	-0.87	0.00	ETHENE + HO. = RO2-R. + RO2. + 1.56 HCHO + 0.22 CCHO
	1.68E-18	9.14E-15	5.13	0.00	ETHENE + O3 = HCHO + (HCHO2)
	2.18E-16	4.39E-13	4.53	2.00	ETHENE + NO3 = R2O2. + RO2. + 2 HCHO + NO2
	7.42E-13	1.04E-11	1.57	0.00	ETHENE + O = RO2-R. + HO2. + RO2. + HCHO + CO
	2.60E-11	4.85E-12	-1.00	0.00	PROPENE + HO. = RO2-R. + RO2. + HCHO + CCHO
	1.05E-17	5.51E-15	3.73	0.00	PROPENE + O3 = 0.6 HCHO + 0.4 CCHO + 0.4 (HCHO2) + 0.6 (CCHO2)
	9.74E-15	4.59E-13	2.30	0.00	PROPENE + NO3 = R2O2. + RO2. + HCHO + CCHO + NO2
	4.01E-12	1.18E-11	0.64	0.00	PROPENE + O = 0.4 HO2. + 0.5 RCHO + 0.5 MEK + -0.5 -C
	6.30E-11	1.01E-11	-1.09	0.00	T-2-BUTE + HO. = RO2-R. + RO2. + 2 CCHO
	1.95E-16	6.64E-15	2.10	0.00	T-2-BUTE + O3 = CCHO + (CCHO2)
	3.92E-13	1.10E-13	-0.76	2.00	T-2-BUTE + NO3 = R2O2. + RO2. + 2 CCHO + NO2
	2.34E-11	2.26E-11	-0.02	0.00	T-2-BUTE + O = 0.4 HO2. + 0.5 RCHO + 0.5 MEK + 0.5 -C
	9.88E-11	2.54E-11	-0.81	0.00	ISOP + HO. = 0.088 RO2-N. + 0.912 RO2-R. + 0.629 HCHO + 0.912 ISOPROD + 0.079 R2O2. + 1.079 RO2. + 0.283 -C
	1.34E-17	7.86E-15	3.80	0.00	ISOP + O3 = 0.4 HCHO + 0.6 ISOPROD + 0.55 (HCHO2) + 0.2 (C:CC(C)O2) + 0.2 (C:C(C)CHO2) + 0.05 -C
	3.60E-11	(No T Dependence)			ISOP + O = 0.75 "ISOPROD + -C" + 0.25 "C2CO-O2. + RCO3. + 2 HCHO + RO2-R. + RO2."
	6.81E-13	3.03E-12	0.89	0.00	ISOP + NO3 = 0.8 "RCHO + RNO3 + RO2-R." + 0.2 "ISOPROD + R2O2. + NO2" + RO2. + -2.2 -C
	1.50E-19	(No T Dependence)			ISOP + NO2 = 0.8 "RCHO + RNO3 + RO2-R." + 0.2 "ISOPROD + R2O2. + NO" + RO2. + -2.2 -C
	5.31E-11	1.21E-11	-0.88	0.00	APIN + HO. = RO2-R. + RCHO + RO2. + 7 -C
	1.00E-16	9.90E-16	1.37	0.00	APIN + O3 = 0.05 HCHO + 0.2 CCHO + 0.5 RCHO + 0.61 MEK + 0.075 CO + 0.05 CCO-O2. + 0.05 C2CO-O2. + 0.1 RCO3. + 0.105 HO2. + 0.16 HO. + 0.135 RO2-R. + 0.15 R2O2. + 0.285 RO2. + 5.285 -C
	6.10E-12	1.19E-12	-0.97	0.00	APIN + NO3 = NO2 + R2O2. + RCHO + RO2. + 7 -C
	3.00E-11	(No T Dependence)			APIN + O = 0.4 HO2. + 0.5 MEK + 0.5 RCHO + 6.5 -C
	6.57E-11	(No T Dependence)			UNKN + HO. = RO2-R. + RO2. + 0.5 HCHO + RCHO + 6.5 -C
	5.85E-17	(No T Dependence)			UNKN + O3 = 0.135 RO2-R. + 0.135 HO2. + 0.075 R2O2. + 0.21 RO2. + 0.025 CCO-O2. + 0.025 C2CO-O2. + 0.05 RCO3. + 0.275 HCHO + 0.175 CCHO + 0.5 RCHO + 0.41 MEK + 0.185 CO + 5.925 -C + 0.11 HO.
	4.30E-12	(No T Dependence)			UNKN + NO3 = R2O2. + RO2. + 0.5 HCHO + RCHO + 6.5 -C + NO2
	2.90E-11	(No T Dependence)			UNKN + O = 0.4 HO2. + 0.5 RCHO + 0.5 MEK + 6.5 -C
	5.91E-12	1.81E-12	-0.70	0.00	TOLUENE + HO. = 0.085 BALD + 0.26 CRES + 0.118 GLY + 0.847 MGLY + 0.276 AFG2 + 0.74 RO2-R. + 0.26 HO2. + 0.981 -C + 0.74 RO2.
	2.36E-11	(No T Dependence)			M-XYLENE + HO. = 0.04 BALD + 0.18 CRES + 0.108 GLY + 1.554 MGLY + 0.505 AFG2 + 0.82 RO2-R. + 0.18 HO2. + 0.068 -C + 0.82 RO2.

Table A-2 (continued)

Rxn.	Kinetic Parameters [a]				Reactions [b]
Label	k(300)	A	Ea	B	
Lumped Species used in EKMA Simulations [c]					
AlOH	3.46E-12	2.56E-12	-0.18	0.00	ALK1 + HO. = 0.911 RO2-R. + 0.074 RO2-N. + 0.005 RO2-XN. + 0.011 HO2. + 0.575 R2O2. + 1.564 RO2. + 0.065 HCHO + 0.339 CCHO + 0.196 RCHO + 0.322 ACET + 0.448 MEK + 0.024 CO + 0.025 GLY + 0.051 -C
A2OH	9.14E-12	5.12E-12	-0.35	0.00	ALK2 + HO. = 0.749 RO2-R. + 0.249 RO2-N. + 0.002 RO2-XN. + 0.891 R2O2. + 1.891 RO2. + 0.029 HCHO + 0.048 CCHO + 0.288 RCHO + 0.028 ACET + 1.105 MEK + 0.043 CO + 0.018 CO2 + 1.268 -C
B1OH	5.87E-12	(No T Dependence)			ARO1 + HO. = 0.742 RO2-R. + 0.258 HO2. + 0.742 RO2. + 0.015 PHEN + 0.244 CRES + 0.08 BALD + 0.124 GLY + 0.681 MGLY + 0.11 AFG1 + 0.244 AFG2 + 1.857 -C
B2OH	3.22E-11	1.20E-11	-0.59	0.00	ARO2 + HO. = 0.82 RO2-R. + 0.18 HO2. + 0.82 RO2. + 0.18 CRES + 0.036 BALD + 0.068 GLY + 1.02 MGLY + 0.532 AFG2 + 2.588 -C
O2OH	3.17E-11	2.22E-12	-1.59	0.00	OLE2 + HO. = 0.858 RO2-R. + 0.142 RO2-N. + RO2. + 0.858 HCHO + 0.252 CCHO + 0.606 RCHO + 1.267 -C
O2O3	1.08E-17	1.42E-15	2.91	0.00	OLE2 + O3 = 0.6 HCHO + 0.635 RCHO + 0.981 -C + 0.4 (HCHO2) + 0.529 (CCHO2) + 0.071 (RCHO2)
O2N3	1.16E-14	1.99E-13	1.69	0.00	OLE2 + NO3 = R2O2. + RO2. + HCHO + 0.294 CCHO + 0.706 RCHO + 1.451 -C + NO2
O2OA	4.11E-12	4.51E-12	0.06	0.00	OLE2 + O = 0.4 HO2. + 0.5 RCHO + 0.5 MEK + 1.657 -C
O3OH	6.23E-11	4.54E-12	-1.56	0.00	OLE3 + HO. = 0.861 RO2-R. + 0.139 RO2-N. + RO2. + 0.24 HCHO + 0.661 CCHO + 0.506 RCHO + 0.113 ACET + 0.086 MEK + 0.057 BALD + 0.848 -C
O3O3	1.70E-16	1.77E-15	1.40	0.00	OLE3 + O3 = 0.203 HCHO + 0.358 CCHO + 0.309 RCHO + 0.061 MEK + 0.027 BALD + 0.976 -C + 0.076 (HCHO2) + 0.409 (CCHO2) + 0.279 (RCHO2) + 0.158 (C(C)CO2 + 0.039 (C(R)CO2 + 0.04 (BZCHO2)
O3N3	1.07E-12	3.19E-13	-0.72	0.00	OLE3 + NO3 = R2O2. + RO2. + 0.278 HCHO + 0.767 CCHO + 0.588 RCHO + 0.131 ACET + 0.1 MEK + 0.066 BALD + 0.871 -C + NO2
O3OA	2.52E-11	8.66E-12	-0.64	0.00	OLE3 + O = 0.4 HO2. + 0.5 RCHO + 0.5 MEK + 2.205 -C
Methyl Acetate (Model A) [d]					
	3.47E-13	8.30E-12	0.52	0.00	ME-ACET + HO. = RO2-R. + R2O2. + 2 HCHO + CO2 + 2 RO2.
Methyl Acetate (Model B) (preferred mechanism)					
	3.47E-13	8.30E-12	0.52	0.00	ME-ACET + HO. = RO2-R. + MEK + -1 -C + RO2.
Reactions used to Represent Chamber-Dependent Processes [e]					
O3W	(varied)	(No T Dependence)			O3 =
N25I	(varied)	(No T Dependence)			N2O5 = 2 NOX-WALL
N25S	(varied)	(No T Dependence)			N2O5 + H2O = 2 NOX-WALL
NO2W	(varied)	(No T Dependence)			NO2 = (yHONO) HONO + (1-yHONO) NOX-WALL
XSHC	(varied)	(No T Dependence)			HO. = HO2.
RSI	(Phot. Set = NO2)				HV + #RS/K1 = HO.
ONO2	(Phot. Set = NO2)				HV + #E-NO2/K1 = NO2 + #-1 NOX-WALL

[a] Except as noted, expression for rate constant is $k = A e^{Ea/RT} (T/300)^B$. Rate constants and A factor are in cm, molecule, sec. units. Units of Ea is kcal mole⁻¹. "Phot Set" means this is a photolysis reaction, with the absorption coefficients and quantum yields given in Table A-3. In addition, if "#(number)" or "#(parameter)" is given as a reactant, then the value of that number or parameter is multiplied by the result in the "rate constant expression" columns to obtain the rate constant used. Furthermore, "#RCOnnn" as a reactant means that the rate constant for the reaction is obtained by multiplying the rate constant given by that for reaction "nn". Thus, the rate constant given is actually an equilibrium constant.

[b] Format of reaction listing same as used in documentation of the detailed mechanism (Carter 1990).
 [c] Rate constants and product yield parameters based on the mixture of species in the base ROG mixture which are being represented.

[d] Not used in atmospheric reactivity simulations because of poor performance in simulating the chamber data.

[e] See Table A-4 for the values of the parameters used for the specific chambers modeled in this study.

Table A-3. Absorption cross sections and quantum yields for photolysis reactions.

WL (nm)	Abs (cm ²)	QY	WL (nm)	Abs (cm ²)	QY	WL (nm)	Abs (cm ²)	QY	WL (nm)	Abs (cm ²)	QY	WL (nm)	Abs (cm ²)	QY
Photolysis File = NO2														
250.0	2.83E-20	1.000	255.0	1.45E-20	1.000	260.0	1.90E-20	1.000	265.0	2.05E-20	1.000	270.0	3.13E-20	1.000
275.0	4.02E-20	1.000	280.0	5.54E-20	1.000	285.0	6.99E-20	1.000	290.0	8.18E-20	0.999	295.0	9.67E-20	0.998
300.0	1.17E-19	0.997	305.0	1.66E-19	0.996	310.0	1.76E-19	0.995	315.0	2.25E-19	0.994	320.0	2.54E-19	0.993
325.0	2.79E-19	0.992	330.0	2.99E-19	0.991	335.0	3.45E-19	0.990	340.0	3.88E-19	0.989	345.0	4.07E-19	0.988
350.0	4.10E-19	0.987	355.0	5.13E-19	0.986	360.0	4.51E-19	0.984	365.0	5.78E-19	0.983	370.0	5.42E-19	0.981
375.0	5.35E-19	0.979	380.0	5.99E-19	0.975	381.0	5.98E-19	0.974	382.0	5.97E-19	0.973	383.0	5.96E-19	0.972
384.0	5.95E-19	0.971	385.0	5.94E-19	0.969	386.0	5.95E-19	0.967	387.0	5.96E-19	0.966	388.0	5.98E-19	0.964
389.0	5.99E-19	0.962	390.0	6.00E-19	0.960	391.0	5.98E-19	0.959	392.0	5.96E-19	0.957	393.0	5.93E-19	0.953
394.0	5.91E-19	0.950	395.0	5.89E-19	0.942	396.0	6.06E-19	0.922	397.0	6.24E-19	0.870	398.0	6.41E-19	0.820
399.0	6.59E-19	0.760	400.0	6.76E-19	0.695	401.0	6.67E-19	0.635	402.0	6.58E-19	0.560	403.0	6.50E-19	0.485
404.0	6.41E-19	0.425	405.0	6.32E-19	0.350	406.0	6.21E-19	0.290	407.0	6.10E-19	0.225	408.0	5.99E-19	0.185
409.0	5.88E-19	0.153	410.0	5.77E-19	0.130	411.0	5.88E-19	0.110	412.0	5.98E-19	0.094	413.0	6.09E-19	0.083
414.0	6.19E-19	0.070	415.0	6.30E-19	0.059	416.0	6.29E-19	0.048	417.0	6.27E-19	0.039	418.0	6.26E-19	0.030
419.0	6.24E-19	0.023	420.0	6.23E-19	0.018	421.0	6.18E-19	0.012	422.0	6.14E-19	0.008	423.0	6.09E-19	0.004
424.0	6.05E-19	0.000	425.0	6.00E-19	0.000									
Photolysis File = NO3NO														
585.0	2.77E-18	0.000	590.0	5.14E-18	0.250	595.0	4.08E-18	0.400	600.0	2.83E-18	0.250	605.0	3.45E-18	0.200
610.0	1.48E-18	0.200	615.0	1.96E-18	0.100	620.0	3.58E-18	0.100	625.0	9.25E-18	0.050	630.0	5.66E-18	0.050
635.0	1.45E-18	0.030	640.0	1.11E-18	0.000									
Photolysis File = NO3NO2														
400.0	0.00E+00	1.000	405.0	3.00E-20	1.000	410.0	4.00E-20	1.000	415.0	5.00E-20	1.000	420.0	8.00E-20	1.000
425.0	1.00E-19	1.000	430.0	1.30E-19	1.000	435.0	1.80E-19	1.000	440.0	1.90E-19	1.000	445.0	2.20E-19	1.000
450.0	2.80E-19	1.000	455.0	3.30E-19	1.000	460.0	3.70E-19	1.000	465.0	4.30E-19	1.000	470.0	5.10E-19	1.000
475.0	6.00E-19	1.000	480.0	6.40E-19	1.000	485.0	6.90E-19	1.000	490.0	8.80E-19	1.000	495.0	9.50E-19	1.000
500.0	1.01E-18	1.000	505.0	1.10E-18	1.000	510.0	1.32E-18	1.000	515.0	1.40E-18	1.000	520.0	1.45E-18	1.000
525.0	1.48E-18	1.000	530.0	1.94E-18	1.000	535.0	2.04E-18	1.000	540.0	1.81E-18	1.000	545.0	1.81E-18	1.000
550.0	2.36E-18	1.000	555.0	2.68E-18	1.000	560.0	3.07E-18	1.000	565.0	2.53E-18	1.000	570.0	2.54E-18	1.000
575.0	2.74E-18	1.000	580.0	3.05E-18	1.000	585.0	2.77E-18	1.000	590.0	5.14E-18	0.750	595.0	4.08E-18	0.600
600.0	2.83E-18	0.550	605.0	3.45E-18	0.400	610.0	1.45E-18	0.300	615.0	1.96E-18	0.250	620.0	3.58E-18	0.200
625.0	9.25E-18	0.150	630.0	5.66E-18	0.050	635.0	1.45E-18	0.000						
Photolysis File = O3O3P														
280.0	3.97E-18	0.100	281.0	3.60E-18	0.100	282.0	3.24E-18	0.100	283.0	3.01E-18	0.100	284.0	2.73E-18	0.100
285.0	2.44E-18	0.100	286.0	2.21E-18	0.100	287.0	2.01E-18	0.100	288.0	1.76E-18	0.100	289.0	1.58E-18	0.100
290.0	1.41E-18	0.100	291.0	1.26E-18	0.100	292.0	1.10E-18	0.100	293.0	9.89E-19	0.100	294.0	8.59E-19	0.100
295.0	7.70E-19	0.100	296.0	6.67E-19	0.100	297.0	5.84E-19	0.100	298.0	5.07E-19	0.100	299.0	4.52E-19	0.100
300.0	3.92E-19	0.100	301.0	3.42E-19	0.100	302.0	3.06E-19	0.100	303.0	2.60E-19	0.100	304.0	2.37E-19	0.100
305.0	2.01E-19	0.112	306.0	1.79E-19	0.149	307.0	1.56E-19	0.197	308.0	1.38E-19	0.259	309.0	1.25E-19	0.339
310.0	1.02E-19	0.437	311.0	9.17E-20	0.546	312.0	7.88E-20	0.652	313.0	6.77E-20	0.743	314.0	6.35E-20	0.816
315.0	5.10E-20	0.872	316.0	4.61E-20	0.916	317.0	4.17E-20	0.949	318.0	3.72E-20	0.976	319.0	2.69E-20	0.997
320.0	3.23E-20	1.000	330.0	6.70E-21	1.000	340.0	1.70E-21	1.000	350.0	4.00E-22	1.000	355.0	0.00E+00	1.000
400.0	0.00E+00	1.000	450.0	1.60E-22	1.000	500.0	1.34E-21	1.000	550.0	3.32E-21	1.000	600.0	5.06E-21	1.000
650.0	2.45E-21	1.000	700.0	8.70E-22	1.000	750.0	3.20E-22	1.000	800.0	1.60E-22	1.000	900.0	0.00E+00	1.000
Photolysis File = O3O1D														
280.0	3.97E-18	0.900	281.0	3.60E-18	0.900	282.0	3.24E-18	0.900	283.0	3.01E-18	0.900	284.0	2.73E-18	0.900
285.0	2.44E-18	0.900	286.0	2.21E-18	0.900	287.0	2.01E-18	0.900	288.0	1.76E-18	0.900	289.0	1.58E-18	0.900
290.0	1.41E-18	0.900	291.0	1.26E-18	0.900	292.0	1.10E-18	0.900	293.0	9.89E-19	0.900	294.0	8.59E-19	0.900
295.0	7.70E-19	0.900	296.0	6.67E-19	0.900	297.0	5.84E-19	0.900	298.0	5.07E-19	0.900	299.0	4.52E-19	0.900
300.0	3.92E-19	0.900	301.0	3.42E-19	0.900	302.0	3.06E-19	0.900	303.0	2.60E-19	0.900	304.0	2.37E-19	0.900
305.0	2.01E-19	0.888	306.0	1.79E-19	0.851	307.0	1.56E-19	0.803	308.0	1.38E-19	0.741	309.0	1.25E-19	0.661
310.0	1.02E-19	0.563	311.0	9.17E-20	0.454	312.0	7.88E-20	0.348	313.0	6.77E-20	0.257	314.0	6.35E-20	0.184
315.0	5.10E-20	0.128	316.0	4.61E-20	0.084	317.0	4.17E-20	0.051	318.0	3.72E-20	0.024	319.0	2.69E-20	0.003
320.0	3.23E-20	0.000												
Photolysis File = HONO														
311.0	0.00E+00	1.000	312.0	2.00E-21	1.000	313.0	4.20E-21	1.000	314.0	4.60E-21	1.000	315.0	4.20E-21	1.000
316.0	3.00E-21	1.000	317.0	4.60E-21	1.000	318.0	3.60E-21	1.000	319.0	6.10E-21	1.000	320.0	2.10E-20	1.000
321.0	4.27E-21	1.000	322.0	4.01E-21	1.000	323.0	3.93E-21	1.000	324.0	4.01E-21	1.000	325.0	4.04E-21	1.000
326.0	3.13E-21	1.000	327.0	4.12E-21	1.000	328.0	7.55E-21	1.000	329.0	6.64E-21	1.000	330.0	7.29E-21	1.000
331.0	8.70E-21	1.000	332.0	1.38E-21	1.000	333.0	5.91E-21	1.000	334.0	5.91E-21	1.000	335.0	6.45E-21	1.000
336.0	5.91E-21	1.000	337.0	4.58E-21	1.000	338.0	1.91E-21	1.000	339.0	1.63E-21	1.000	340.0	1.05E-21	1.000
341.0	8.70E-21	1.000	342.0	3.35E-21	1.000	343.0	2.01E-21	1.000	344.0	1.02E-21	1.000	345.0	8.54E-21	1.000
346.0	8.32E-21	1.000	347.0	8.20E-21	1.000	348.0	7.49E-21	1.000	349.0	7.13E-21	1.000	350.0	6.83E-21	1.000
351.0	1.74E-21	1.000	352.0	1.14E-21	1.000	353.0	3.71E-21	1.000	354.0	4.96E-21	1.000	355.0	2.46E-21	1.000
356.0	1.19E-21	1.000	357.0	9.35E-21	1.000	358.0	7.78E-21	1.000	359.0	7.29E-21	1.000	360.0	6.83E-21	1.000
361.0	6.90E-21	1.000	362.0	7.32E-21	1.000	363.0	9.00E-21	1.000	364.0	1.21E-21	1.000	365.0	1.33E-21	1.000
366.0	2.13E-21	1.000	367.0	3.52E-21	1.000	368.0	4.50E-21	1.000	369.0	2.93E-21	1.000	370.0	1.19E-21	1.000
371.0	9.46E-21	1.000	372.0	8.85E-21	1.000	373.0	7.44E-21	1.000	374.0	4.77E-21	1.000	375.0	2.70E-21	1.000
376.0	1.90E-21	1.000	377.0	1.50E-21	1.000	378.0	1.90E-21	1.000	379.0	5.80E-21	1.000	380.0	7.78E-21	1.000
381.0	1.14E-21	1.000	382.0	1.40E-21	1.000	383.0	1.72E-21	1.000	384.0	1.99E-21	1.000	385.0	1.90E-21	1.000
386.0	1.19E-21	1.000	387.0	5.65E-21	1.000	388.0	3.20E-21	1.000	389.0	1.90E-21	1.000	390.0	1.20E-21	1.000
391.0	5.00E-21	1.000	392.0	0.00E+00	1.000									
Photolysis File = H2O2														
250.0	8.30E-20	1.000	255.0	6.70E-20	1.000	260.0	5.20E-20	1.000	265.0	4.20E-20	1.000	270.0	3.20E-20	1.000
275.0	2.50E-20	1.000	280.0	2.00E-20	1.000	285.0	1.50E-20	1.000	290.0	1.13E-20	1.000	295.0	8.70E-21	1.000
300.0	6.60E-21	1.000	305.0	4.90E-21	1.000	310.0	3.70E-21	1.000	315.0	2.80E-21	1.000	320.0	2.00E-21	1.000
325.0	1.50E-21	1.000	330.0	1.20E-21	1.000	335.0	9.00E-22	1.000	340.0	7.00E-22	1.000	345.0	5.00E-22	1.000
350.0	3.00E-22	1.000	355.0	0.00E+00	1.000									

Table A-3. (continued)

WL (nm)	Abs (cm ²)	QY	WL (nm)	Abs (cm ²)	QY	WL (nm)	Abs (cm ²)	QY	WL (nm)	Abs (cm ²)	QY	WL (nm)	Abs (cm ²)	QY
Photolysis File = CO2H														
210.0	3.75E-19	1.000	220.0	2.20E-19	1.000	230.0	1.38E-19	1.000	240.0	8.80E-20	1.000	250.0	5.80E-20	1.000
260.0	3.80E-20	1.000	270.0	2.50E-20	1.000	280.0	1.50E-20	1.000	290.0	9.00E-21	1.000	300.0	5.80E-21	1.000
310.0	3.40E-21	1.000	320.0	1.90E-21	1.000	330.0	1.10E-21	1.000	340.0	6.00E-22	1.000	350.0	4.00E-22	1.000
360.0	0.00E+00	1.000												
Photolysis File = HCHONEWR														
280.0	2.49E-20	0.590	280.5	1.42E-20	0.596	281.0	1.51E-20	0.602	281.5	1.32E-20	0.608	282.0	9.73E-21	0.614
282.5	6.76E-21	0.620	283.0	5.82E-21	0.626	283.5	9.10E-21	0.632	284.0	3.71E-20	0.638	284.5	4.81E-20	0.644
285.0	3.95E-20	0.650	285.5	2.87E-20	0.656	286.0	2.24E-20	0.662	286.5	1.74E-20	0.668	287.0	1.13E-20	0.674
287.5	1.10E-20	0.680	288.0	2.62E-20	0.686	288.5	4.00E-20	0.692	289.0	3.55E-20	0.698	289.5	2.12E-20	0.704
290.0	1.07E-20	0.710	290.5	1.35E-20	0.713	291.0	1.99E-20	0.717	291.5	1.56E-20	0.721	292.0	8.65E-21	0.724
292.5	5.90E-21	0.727	293.0	1.11E-20	0.731	293.5	6.26E-20	0.735	294.0	7.40E-20	0.738	294.5	5.36E-20	0.741
295.0	4.17E-20	0.745	295.5	3.51E-20	0.749	296.0	2.70E-20	0.752	296.5	1.75E-20	0.755	297.0	1.16E-20	0.759
297.5	1.51E-20	0.763	298.0	3.69E-20	0.766	298.5	4.40E-20	0.769	299.0	3.44E-20	0.773	299.5	2.02E-20	0.776
300.0	1.06E-20	0.780	300.4	7.01E-21	0.780	300.6	8.63E-21	0.779	300.8	1.47E-20	0.779	301.0	2.01E-20	0.779
301.2	2.17E-20	0.779	301.4	1.96E-20	0.779	301.6	1.54E-20	0.778	301.8	1.26E-20	0.778	302.0	1.03E-20	0.778
302.2	8.53E-21	0.778	302.4	7.13E-21	0.778	302.6	6.61E-21	0.777	302.8	1.44E-20	0.777	303.0	3.18E-20	0.777
303.2	3.81E-20	0.777	303.4	5.57E-20	0.777	303.6	6.91E-20	0.776	303.8	6.58E-20	0.776	304.0	6.96E-20	0.776
304.2	5.79E-20	0.776	304.4	5.24E-20	0.776	304.6	4.30E-20	0.775	304.8	3.28E-20	0.775	305.0	3.60E-20	0.775
305.2	5.12E-20	0.775	305.4	4.77E-20	0.775	305.6	4.43E-20	0.774	305.8	4.60E-20	0.774	306.0	4.01E-20	0.774
306.2	3.28E-20	0.774	306.4	2.66E-20	0.774	306.6	2.42E-20	0.773	306.8	1.95E-20	0.773	307.0	1.58E-20	0.773
307.2	1.37E-20	0.773	307.4	1.19E-20	0.773	307.6	1.01E-20	0.772	307.8	9.01E-21	0.772	308.0	8.84E-21	0.772
308.2	2.08E-20	0.772	308.4	2.39E-20	0.772	308.6	3.08E-20	0.771	308.8	3.39E-20	0.771	309.0	3.18E-20	0.771
309.2	3.06E-20	0.771	309.4	2.84E-20	0.771	309.6	2.46E-20	0.770	309.8	1.95E-20	0.770	310.0	1.57E-20	0.770
310.2	1.26E-20	0.767	310.4	9.26E-21	0.764	310.6	7.71E-21	0.761	310.8	6.05E-21	0.758	311.0	5.13E-21	0.755
311.2	4.82E-21	0.752	311.4	4.54E-21	0.749	311.6	6.81E-21	0.746	311.8	1.04E-20	0.743	312.0	1.43E-20	0.740
312.2	1.47E-20	0.737	312.4	1.35E-20	0.734	312.6	1.13E-20	0.731	312.8	9.86E-21	0.728	313.0	7.82E-21	0.725
313.2	6.48E-21	0.722	313.4	1.07E-20	0.719	313.6	2.39E-20	0.716	313.8	3.80E-20	0.713	314.0	5.76E-20	0.710
314.2	6.14E-20	0.707	314.4	7.45E-20	0.704	314.6	5.78E-20	0.701	314.8	5.59E-20	0.698	315.0	4.91E-20	0.695
315.2	4.37E-20	0.692	315.4	3.92E-20	0.689	315.6	2.89E-20	0.686	315.8	2.82E-20	0.683	316.0	2.10E-20	0.680
316.2	1.66E-20	0.677	316.4	2.05E-20	0.674	316.6	4.38E-20	0.671	316.8	5.86E-20	0.668	317.0	6.28E-20	0.665
317.2	5.07E-20	0.662	317.4	4.33E-20	0.659	317.6	4.17E-20	0.656	317.8	3.11E-20	0.653	318.0	2.64E-20	0.650
318.2	2.24E-20	0.647	318.4	1.70E-20	0.644	318.6	1.24E-20	0.641	318.8	1.11E-20	0.638	319.0	7.70E-21	0.635
319.2	6.36E-21	0.632	319.4	5.36E-21	0.629	319.6	4.79E-21	0.626	319.8	6.48E-21	0.623	320.0	1.48E-20	0.620
320.2	1.47E-20	0.614	320.4	1.36E-20	0.608	320.6	1.69E-20	0.601	320.8	1.32E-20	0.595	321.0	1.49E-20	0.589
321.2	1.17E-20	0.583	321.4	1.15E-20	0.577	321.6	9.64E-21	0.570	321.8	7.26E-21	0.564	322.0	5.94E-21	0.558
322.2	4.13E-21	0.552	322.4	3.36E-21	0.546	322.6	2.39E-21	0.539	322.8	2.01E-21	0.533	323.0	1.76E-21	0.527
323.2	2.82E-21	0.521	323.4	4.65E-21	0.515	323.6	7.00E-21	0.508	323.8	7.80E-21	0.502	324.0	7.87E-21	0.496
324.2	6.59E-21	0.490	324.4	5.60E-21	0.484	324.6	4.66E-21	0.477	324.8	4.21E-21	0.471	325.0	7.77E-21	0.465
325.2	2.15E-20	0.459	325.4	3.75E-20	0.453	325.6	4.10E-20	0.446	325.8	6.47E-20	0.440	326.0	7.59E-20	0.434
326.2	6.51E-20	0.428	326.4	5.53E-20	0.422	326.6	5.76E-20	0.415	326.8	4.43E-20	0.409	327.0	3.44E-20	0.403
327.2	3.22E-20	0.397	327.4	2.13E-20	0.391	327.6	1.91E-20	0.384	327.8	1.42E-20	0.378	328.0	9.15E-21	0.372
328.2	6.79E-21	0.366	328.4	4.99E-21	0.360	328.6	4.77E-21	0.353	328.8	1.75E-20	0.347	329.0	3.27E-20	0.341
329.2	3.99E-20	0.335	329.4	5.13E-20	0.329	329.6	4.00E-20	0.322	329.8	3.61E-20	0.316	330.0	3.38E-20	0.310
330.2	3.08E-20	0.304	330.4	2.16E-20	0.298	330.6	2.09E-20	0.291	330.8	1.41E-20	0.285	331.0	9.95E-21	0.279
331.2	7.76E-21	0.273	331.4	6.16E-21	0.267	331.6	4.06E-21	0.260	331.8	3.03E-21	0.254	332.0	2.41E-21	0.248
332.2	1.74E-21	0.242	332.4	1.33E-21	0.236	332.6	2.70E-21	0.229	332.8	1.65E-21	0.223	333.0	1.17E-21	0.217
333.2	9.84E-22	0.211	333.4	8.52E-22	0.205	333.6	6.32E-22	0.198	333.8	5.21E-22	0.192	334.0	1.46E-21	0.186
334.2	1.80E-21	0.180	334.4	1.43E-21	0.174	334.6	1.03E-21	0.167	334.8	7.19E-22	0.161	335.0	4.84E-22	0.155
335.2	2.73E-22	0.149	335.4	1.34E-22	0.143	335.6	1.62E-22	0.136	335.8	1.25E-22	0.130	336.0	4.47E-22	0.124
336.2	1.23E-21	0.118	336.4	2.02E-21	0.112	336.6	3.00E-21	0.105	336.8	2.40E-21	0.099	337.0	3.07E-21	0.093
337.2	2.29E-21	0.087	337.4	2.46E-21	0.081	337.6	2.92E-21	0.074	337.8	8.10E-21	0.068	338.0	1.82E-20	0.062
338.2	3.10E-20	0.056	338.4	3.24E-20	0.050	338.6	4.79E-20	0.043	338.8	5.25E-20	0.037	339.0	5.85E-20	0.031
339.2	4.33E-20	0.025	339.4	4.20E-20	0.019	339.6	3.99E-20	0.012	339.8	3.11E-20	0.006	340.0	2.72E-20	0.000
Photolysis File = HCHONEWM														
280.0	2.49E-20	0.350	280.5	1.42E-20	0.346	281.0	1.51E-20	0.341	281.5	1.32E-20	0.336	282.0	9.73E-21	0.332
282.5	6.76E-21	0.327	283.0	5.82E-21	0.323	283.5	9.10E-21	0.319	284.0	3.71E-20	0.314	284.5	4.81E-20	0.309
285.0	3.95E-20	0.305	285.5	2.87E-20	0.301	286.0	2.24E-20	0.296	286.5	1.74E-20	0.291	287.0	1.13E-20	0.287
287.5	1.10E-20	0.282	288.0	2.62E-20	0.278	288.5	4.00E-20	0.273	289.0	3.55E-20	0.269	289.5	2.12E-20	0.264
290.0	1.07E-20	0.260	290.5	1.35E-20	0.258	291.0	1.99E-20	0.256	291.5	1.56E-20	0.254	292.0	8.65E-21	0.252
292.5	5.90E-21	0.250	293.0	1.11E-20	0.248	293.5	6.26E-20	0.246	294.0	7.40E-20	0.244	294.5	5.36E-20	0.242
295.0	4.17E-20	0.240	295.5	3.51E-20	0.238	296.0	2.70E-20	0.236	296.5	1.75E-20	0.234	297.0	1.16E-20	0.232
297.5	1.51E-20	0.230	298.0	3.69E-20	0.228	298.5	4.40E-20	0.226	299.0	3.44E-20	0.224	299.5	2.02E-20	0.222
300.0	1.06E-20	0.220	300.4	7.01E-21	0.220	300.6	8.63E-21	0.221	300.8	1.47E-20	0.221	301.0	2.01E-20	0.221
301.2	2.17E-20	0.221	301.4	1.96E-20	0.221	301.6	1.54E-20	0.222	301.8	1.26E-20	0.222	302.0	1.03E-20	0.222
302.2	8.53E-21	0.222	302.4	7.13E-21	0.222	302.6	6.61E-21	0.223	302.8	1.44E-20	0.223	303.0	3.18E-20	0.223
303.2	3.81E-20	0.223	303.4	5.57E-20	0.223	303.6	6.91E-20	0.224	303.8	6.58E-20	0.224	304.0	6.96E-20	0.224
304.2	5.79E-20	0.224	304.4	5.24E-20	0.224	304.6	4.30E-20	0.225	304.8	3.28E-20	0.225	305.0	3.60E-20	0.225
305.2	5.12E-20	0.225	305.4	4.77E-20	0.225	305.6	4.43E-20	0.226	305.8	4.60E-20	0.226	306.0	4.01E-20	0.226
306.2	3.28E-20	0.226	306.4	2.66E-20	0.226	306.6	2.42E-20	0.227	306.8	1.95E-20	0.227	307.0	1.58E-20	0.227
307.2	1.37E-20	0.227	307.4	1.19E-20	0.227	307.6	1.01E-20	0.228	307.8	9.01E-21	0.228	308.0	8.84E-21	0.228
308.2	2.08E-20	0.228	308.4	2.39E-20										

Table A-3. (continued)

WL (nm)	Abs (cm ²)	QY	WL (nm)	Abs (cm ²)	QY	WL (nm)	Abs (cm ²)	QY	WL (nm)	Abs (cm ²)	QY	WL (nm)	Abs (cm ²)	QY
322.2	4.13E-21	0.448	322.4	3.36E-21	0.454	322.6	2.39E-21	0.461	322.8	2.01E-21	0.467	323.0	1.76E-21	0.473
323.2	2.82E-21	0.479	323.4	4.65E-21	0.485	323.6	7.00E-21	0.492	323.8	7.80E-21	0.498	324.0	7.87E-21	0.504
324.2	6.59E-21	0.510	324.4	5.60E-21	0.516	324.6	4.66E-21	0.523	324.8	4.21E-21	0.529	325.0	4.77E-21	0.535
325.2	2.15E-20	0.541	325.4	3.75E-20	0.547	325.6	4.10E-20	0.554	325.8	6.47E-20	0.560	326.0	7.59E-20	0.566
326.2	6.51E-20	0.572	326.4	5.53E-20	0.578	326.6	5.76E-20	0.585	326.8	4.43E-20	0.591	327.0	3.44E-20	0.597
327.2	3.22E-20	0.603	327.4	2.13E-20	0.609	327.6	1.91E-20	0.616	327.8	1.42E-20	0.622	328.0	9.15E-21	0.628
328.2	6.79E-21	0.634	328.4	4.99E-21	0.640	328.6	4.77E-21	0.647	328.8	1.75E-20	0.653	329.0	3.27E-20	0.659
329.2	3.99E-20	0.665	329.4	5.13E-20	0.671	329.6	4.00E-20	0.678	329.8	3.61E-20	0.684	330.0	3.38E-20	0.690
330.2	3.08E-20	0.694	330.4	2.16E-20	0.699	330.6	2.09E-20	0.703	330.8	1.41E-20	0.708	331.0	9.95E-21	0.712
331.2	7.76E-21	0.717	331.4	6.16E-21	0.721	331.6	4.06E-21	0.726	331.8	3.03E-21	0.730	332.0	2.41E-21	0.735
332.2	1.74E-21	0.739	332.4	1.33E-21	0.744	332.6	2.70E-21	0.748	332.8	1.65E-21	0.753	333.0	1.17E-21	0.757
333.2	9.84E-22	0.762	333.4	8.52E-22	0.766	333.6	6.32E-22	0.771	333.8	5.21E-22	0.775	334.0	4.46E-21	0.780
334.2	1.80E-21	0.784	334.4	1.43E-21	0.789	334.6	1.03E-21	0.793	334.8	7.19E-22	0.798	335.0	4.84E-22	0.802
335.2	2.73E-22	0.798	335.4	1.34E-22	0.794	335.6	0.00E+00	0.790	335.8	1.25E-22	0.786	336.0	4.47E-22	0.782
336.2	1.23E-21	0.778	336.4	2.02E-21	0.773	336.6	3.00E-21	0.769	336.8	2.40E-21	0.764	337.0	3.07E-21	0.759
337.2	2.29E-21	0.754	337.4	2.46E-21	0.749	337.6	2.92E-21	0.745	337.8	8.10E-21	0.740	338.0	1.82E-20	0.734
338.2	3.10E-20	0.729	338.4	3.24E-20	0.724	338.6	4.79E-20	0.719	338.8	5.25E-20	0.714	339.0	5.85E-20	0.709
339.2	4.33E-20	0.703	339.4	4.20E-20	0.698	339.6	3.99E-20	0.693	339.8	3.11E-20	0.687	340.0	2.72E-20	0.682
340.2	1.99E-20	0.676	340.4	1.76E-20	0.671	340.6	1.39E-20	0.666	340.8	1.01E-20	0.660	341.0	6.57E-21	0.655
341.2	4.83E-21	0.649	341.4	3.47E-21	0.643	341.6	2.23E-21	0.638	341.8	1.55E-21	0.632	342.0	3.70E-21	0.627
342.2	4.64E-21	0.621	342.4	1.08E-20	0.616	342.6	1.14E-20	0.610	342.8	1.79E-20	0.604	343.0	2.33E-20	0.599
343.2	1.72E-20	0.593	343.4	1.55E-20	0.588	343.6	1.46E-20	0.582	343.8	1.38E-20	0.576	344.0	1.00E-20	0.571
344.2	8.26E-21	0.565	344.4	6.32E-21	0.559	344.6	4.28E-21	0.554	344.8	3.22E-21	0.548	345.0	2.54E-21	0.542
345.2	1.60E-21	0.537	345.4	1.15E-21	0.531	345.6	8.90E-22	0.525	345.8	6.50E-22	0.520	346.0	5.09E-22	0.514
346.2	5.15E-22	0.508	346.4	3.45E-22	0.503	346.6	3.18E-22	0.497	346.8	3.56E-22	0.491	347.0	3.24E-22	0.485
347.2	3.34E-22	0.480	347.4	2.88E-22	0.474	347.6	2.84E-22	0.468	347.8	9.37E-22	0.463	348.0	9.70E-22	0.457
348.2	7.60E-22	0.451	348.4	6.24E-22	0.446	348.6	4.99E-22	0.440	348.8	4.08E-22	0.434	349.0	3.39E-22	0.428
349.2	1.64E-22	0.423	349.4	1.49E-22	0.417	349.6	8.30E-23	0.411	349.8	2.52E-23	0.406	350.0	2.59E-23	0.400
350.2	0.00E+00	0.394	350.4	5.16E-23	0.389	350.6	0.00E+00	0.383	350.8	2.16E-23	0.377	351.0	7.07E-23	0.371
351.2	3.45E-23	0.366	351.4	1.97E-22	0.360	351.6	4.80E-22	0.354	351.8	3.13E-21	0.349	352.0	6.41E-21	0.343
352.2	8.38E-21	0.337	352.4	1.55E-20	0.331	352.6	1.86E-20	0.326	352.8	1.94E-20	0.320	353.0	2.78E-20	0.314
353.2	1.96E-20	0.309	353.4	1.67E-20	0.303	353.6	1.75E-20	0.297	353.8	1.63E-20	0.291	354.0	1.36E-20	0.286
354.2	1.07E-20	0.280	354.4	9.82E-21	0.274	354.6	8.66E-21	0.269	354.8	6.44E-21	0.263	355.0	4.84E-21	0.257
355.2	3.49E-21	0.251	355.4	2.41E-21	0.246	355.6	1.74E-21	0.240	355.8	1.11E-21	0.234	356.0	7.37E-22	0.229
356.2	4.17E-22	0.223	356.4	1.95E-22	0.217	356.6	1.50E-22	0.211	356.8	8.14E-23	0.206	357.0	0.00E+00	0.200
Photolysis File = CCHOR														
260.0	2.00E-20	0.310	270.0	3.40E-20	0.390	280.0	4.50E-20	0.580	290.0	4.90E-20	0.530	295.0	4.50E-20	0.480
300.0	4.30E-20	0.430	305.0	3.40E-20	0.370	315.0	2.10E-20	0.170	320.0	1.80E-20	0.100	325.0	1.10E-20	0.040
330.0	6.90E-21	0.000												
Photolysis File = RCHO														
280.0	5.26E-20	0.960	290.0	5.77E-20	0.910	300.0	5.05E-20	0.860	310.0	3.68E-20	0.600	320.0	1.66E-20	0.360
330.0	6.49E-21	0.200	340.0	1.44E-21	0.080	345.0	0.00E+00	0.020						
Photolysis File = ACET-93C														
250.0	2.37E-20	0.760	260.0	3.66E-20	0.800	270.0	4.63E-20	0.640	280.0	5.05E-20	0.550	290.0	4.21E-20	0.300
300.0	2.78E-20	0.150	310.0	1.44E-20	0.050	320.0	4.80E-21	0.026	330.0	8.00E-22	0.017	340.0	1.00E-22	0.000
350.0	3.00E-23	0.000	360.0	0.00E+00	0.000									
Photolysis File = KETONE														
210.0	1.10E-21	1.000	220.0	1.20E-21	1.000	230.0	4.60E-21	1.000	240.0	1.30E-20	1.000	250.0	2.68E-20	1.000
260.0	4.21E-20	1.000	270.0	5.54E-20	1.000	280.0	5.92E-20	1.000	290.0	5.16E-20	1.000	300.0	3.44E-20	1.000
310.0	1.53E-20	1.000	320.0	4.60E-21	1.000	330.0	1.10E-21	1.000	340.0	0.00E+00	1.000			
Photolysis File = GLYOXAL1														
230.0	2.87E-21	1.000	235.0	2.87E-21	1.000	240.0	4.30E-21	1.000	245.0	5.73E-21	1.000	250.0	8.60E-21	1.000
255.0	1.15E-20	1.000	260.0	1.43E-20	1.000	265.0	1.86E-20	1.000	270.0	2.29E-20	1.000	275.0	2.58E-20	1.000
280.0	2.87E-20	1.000	285.0	3.30E-20	1.000	290.0	3.15E-20	1.000	295.0	3.30E-20	1.000	300.0	3.58E-20	1.000
305.0	2.72E-20	1.000	310.0	2.72E-20	1.000	312.5	2.87E-20	1.000	315.0	2.29E-20	1.000	320.0	1.43E-20	1.000
325.0	1.15E-20	1.000	327.5	1.43E-20	1.000	330.0	1.15E-20	1.000	335.0	2.87E-21	1.000	340.0	0.00E+00	1.000
Photolysis File = GLYOXAL2														
355.0	0.00E+00	1.000	360.0	2.29E-21	1.000	365.0	2.87E-21	1.000	370.0	8.03E-21	1.000	375.0	1.00E-20	1.000
380.0	1.72E-20	1.000	382.0	1.58E-20	1.000	384.0	1.49E-20	1.000	386.0	1.49E-20	1.000	388.0	2.87E-20	1.000
390.0	3.15E-20	1.000	391.0	3.24E-20	1.000	392.0	3.04E-20	1.000	393.0	2.23E-20	1.000	394.0	2.63E-20	1.000
395.0	3.04E-20	1.000	396.0	2.63E-20	1.000	397.0	2.43E-20	1.000	398.0	3.24E-20	1.000	399.0	3.04E-20	1.000
400.0	2.84E-20	1.000	401.0	3.24E-20	1.000	402.0	4.46E-20	1.000	403.0	5.27E-20	1.000	404.0	4.26E-20	1.000
405.0	3.04E-20	1.000	406.0	3.04E-20	1.000	407.0	2.84E-20	1.000	408.0	2.43E-20	1.000	409.0	2.84E-20	1.000
410.0	6.08E-20	1.000	411.0	5.07E-20	1.000	411.5	6.08E-20	1.000	412.0	4.86E-20	1.000	413.0	8.31E-20	1.000
413.5	6.48E-20	1.000	414.0	7.50E-20	1.000	414.5	8.11E-20	1.000	415.0	8.11E-20	1.000	415.5	6.89E-20	1.000
416.0	4.26E-20	1.000	417.0	4.86E-20	1.000	418.0	5.88E-20	1.000	419.0	6.69E-20	1.000	420.0	3.85E-20	1.000
421.0	5.67E-20	1.000	421.5	4.46E-20	1.000	422.0	5.27E-20	1.000	422.5	1.05E-19	1.000	423.0	8.51E-20	1.000
424.0	6.08E-20	1.000	425.0	7.29E-20	1.000	426.0	1.18E-19	1.000	426.5	1.30E-19	1.000	427.0	1.07E-19	1.000
428.0	1.66E-19	1.000	429.0	4.05E-20	1.000	430.0	5.07E-20	1.000	431.0	4.86E-20	1.000	432.0	4.05E-20	1.000
433.0	3.65E-20	1.000	434.0	4.05E-20	1.000	434.5	6.08E-20	1.000	435.0	5.07E-20	1.000	436.0	8.11E-20	1.000
436.5	1.13E-19	1.000	437.0	5.27E-20	1.000	438.0	1.01E-19	1.000	438.5	1.38E-19	1.000	439.0	7.70E-20	1.000
440.0	2.47E-19	1.000	441.0	8.11E-20	1.000	442.0	6.08E-20	1.000	443.0	7.50E-20	1.000	444.0	9.32E-20	1.000
445.0	1.13E-19	1.000	446.0	5.27E-20	1.000	447.0	2.43E-20	1.000	448.0	2.84E-20	1.000	449.0	3.85E-20	1.000
450.0	6.08E-20	1.000	451.0	1.09E-19	1.000	451.5	9.32E-20	1.000	452.0	1.22E-19	1.000	453.0	2.39E-19	1.000
454.0	1.70E-19	1.000	455.0	3.40E-19	1.000	455.5	4.05E-19	1.000	456.0	1.01E-19	1.000	457.0	1.62E-20	1.000
458.0	1.22E-20	1.000	458.5	1.42E-20	1.000	459.0	4.05E-21	1.000	460.0	4.05E-21	1.000	460.5	6.08E-21	1.000
461.0	2.03E-21	1.000	462.0	0.00E+00	1.000									
Photolysis File = MEGLYOX1														
220.0	2.10E-21	1.000	225.0	2.10E-21	1.000	230.0	4.21E-21	1.000	235.0	7.				

Table A-3. (continued)

WL (nm)	Abs (cm ²)	QY	WL (nm)	Abs (cm ²)	QY	WL (nm)	Abs (cm ²)	QY	WL (nm)	Abs (cm ²)	QY	WL (nm)	Abs (cm ²)	QY
270.0	1.26E-20	1.000	275.0	1.43E-20	1.000	280.0	1.51E-20	1.000	285.0	1.43E-20	1.000	290.0	1.47E-20	1.000
295.0	1.18E-20	1.000	300.0	1.14E-20	1.000	305.0	9.25E-21	1.000	310.0	6.31E-21	1.000	315.0	5.47E-21	1.000
320.0	3.36E-21	1.000	325.0	1.68E-21	1.000	330.0	8.41E-22	1.000	335.0	0.00E+00	1.000			
Photolysis File = MEGLYOX2														
350.0	0.00E+00	1.000	354.0	4.21E-22	1.000	358.0	1.26E-21	1.000	360.0	2.10E-21	1.000	362.0	2.10E-21	1.000
364.0	2.94E-21	1.000	366.0	3.36E-21	1.000	368.0	4.21E-21	1.000	370.0	5.47E-21	1.000	372.0	5.89E-21	1.000
374.0	7.57E-21	1.000	376.0	7.99E-21	1.000	378.0	8.83E-21	1.000	380.0	1.01E-20	1.000	382.0	1.09E-20	1.000
384.0	1.35E-20	1.000	386.0	1.51E-20	1.000	388.0	1.72E-20	1.000	390.0	2.06E-20	1.000	392.0	2.10E-20	1.000
394.0	2.31E-20	1.000	396.0	2.48E-20	1.000	398.0	2.61E-20	1.000	400.0	2.78E-20	1.000	402.0	2.99E-20	1.000
404.0	3.20E-20	1.000	406.0	3.79E-20	1.000	408.0	3.95E-20	1.000	410.0	4.33E-20	1.000	412.0	4.71E-20	1.000
414.0	4.79E-20	1.000	416.0	4.88E-20	1.000	418.0	5.05E-20	1.000	420.0	5.21E-20	1.000	422.0	5.30E-20	1.000
424.0	5.17E-20	1.000	426.0	5.30E-20	1.000	428.0	5.21E-20	1.000	430.0	5.55E-20	1.000	432.0	5.13E-20	1.000
434.0	5.68E-20	1.000	436.0	6.22E-20	1.000	438.0	6.06E-20	1.000	440.0	5.47E-20	1.000	441.0	6.14E-20	1.000
442.0	5.47E-20	1.000	443.0	5.55E-20	1.000	443.5	6.81E-20	1.000	444.0	5.97E-20	1.000	445.0	5.13E-20	1.000
446.0	4.88E-20	1.000	447.0	5.72E-20	1.000	448.0	5.47E-20	1.000	449.0	6.56E-20	1.000	450.0	5.05E-20	1.000
451.0	3.03E-20	1.000	452.0	4.29E-20	1.000	453.0	2.78E-20	1.000	454.0	2.27E-20	1.000	456.0	1.77E-20	1.000
458.0	8.41E-21	1.000	460.0	4.21E-21	1.000	464.0	1.68E-21	1.000	468.0	0.00E+00	1.000			
Photolysis File = BZCHO														
299.0	1.78E-19	1.000	304.0	7.40E-20	1.000	306.0	6.91E-20	1.000	309.0	6.41E-20	1.000	313.0	6.91E-20	1.000
314.0	6.91E-20	1.000	318.0	6.41E-20	1.000	325.0	8.39E-20	1.000	332.0	7.65E-20	1.000	338.0	8.88E-20	1.000
342.0	8.88E-20	1.000	346.0	7.89E-20	1.000	349.0	7.89E-20	1.000	354.0	9.13E-20	1.000	355.0	8.14E-20	1.000
364.0	5.67E-20	1.000	368.0	6.66E-20	1.000	369.0	8.39E-20	1.000	370.0	8.39E-20	1.000	372.0	3.45E-20	1.000
374.0	3.21E-20	1.000	376.0	2.47E-20	1.000	377.0	2.47E-20	1.000	380.0	3.58E-20	1.000	382.0	9.90E-21	1.000
386.0	0.00E+00	1.000												
Photolysis File = ACRROLEIN														
250.0	1.80E-21	1.000	252.0	2.05E-21	1.000	253.0	2.20E-21	1.000	254.0	2.32E-21	1.000	255.0	2.45E-21	1.000
256.0	2.56E-21	1.000	257.0	2.65E-21	1.000	258.0	2.74E-21	1.000	259.0	2.83E-21	1.000	260.0	2.98E-21	1.000
261.0	3.24E-21	1.000	262.0	3.47E-21	1.000	263.0	3.58E-21	1.000	264.0	3.93E-21	1.000	265.0	4.67E-21	1.000
266.0	5.10E-21	1.000	267.0	5.38E-21	1.000	268.0	5.73E-21	1.000	269.0	6.13E-21	1.000	270.0	6.64E-21	1.000
271.0	7.20E-21	1.000	272.0	7.77E-21	1.000	273.0	8.37E-21	1.000	274.0	8.94E-21	1.000	275.0	9.55E-21	1.000
276.0	1.04E-20	1.000	277.0	1.12E-20	1.000	278.0	1.19E-20	1.000	279.0	1.27E-20	1.000	280.0	1.27E-20	1.000
281.0	1.26E-20	1.000	282.0	1.26E-20	1.000	283.0	1.28E-20	1.000	284.0	1.33E-20	1.000	285.0	1.38E-20	1.000
286.0	1.44E-20	1.000	287.0	1.50E-20	1.000	288.0	1.57E-20	1.000	289.0	1.63E-20	1.000	290.0	1.71E-20	1.000
291.0	1.78E-20	1.000	292.0	1.86E-20	1.000	293.0	1.95E-20	1.000	294.0	2.05E-20	1.000	295.0	2.15E-20	1.000
296.0	2.26E-20	1.000	297.0	2.37E-20	1.000	298.0	2.48E-20	1.000	299.0	2.60E-20	1.000	300.0	2.73E-20	1.000
301.0	2.85E-20	1.000	302.0	2.99E-20	1.000	303.0	3.13E-20	1.000	304.0	3.27E-20	1.000	305.0	3.39E-20	1.000
306.0	3.51E-20	1.000	307.0	3.63E-20	1.000	308.0	3.77E-20	1.000	309.0	3.91E-20	1.000	310.0	4.07E-20	1.000
311.0	4.25E-20	1.000	312.0	4.39E-20	1.000	313.0	4.44E-20	1.000	314.0	4.50E-20	1.000	315.0	4.59E-20	1.000
316.0	4.75E-20	1.000	317.0	4.90E-20	1.000	318.0	5.05E-20	1.000	319.0	5.19E-20	1.000	320.0	5.31E-20	1.000
321.0	5.43E-20	1.000	322.0	5.52E-20	1.000	323.0	5.60E-20	1.000	324.0	5.67E-20	1.000	325.0	5.67E-20	1.000
326.0	5.62E-20	1.000	327.0	5.63E-20	1.000	328.0	5.71E-20	1.000	329.0	5.76E-20	1.000	330.0	5.80E-20	1.000
331.0	5.95E-20	1.000	332.0	6.23E-20	1.000	333.0	6.39E-20	1.000	334.0	6.38E-20	1.000	335.0	6.24E-20	1.000
336.0	6.01E-20	1.000	337.0	5.79E-20	1.000	338.0	5.63E-20	1.000	339.0	5.56E-20	1.000	340.0	5.52E-20	1.000
341.0	5.54E-20	1.000	342.0	5.53E-20	1.000	343.0	5.47E-20	1.000	344.0	5.41E-20	1.000	345.0	5.40E-20	1.000
346.0	5.48E-20	1.000	347.0	5.90E-20	1.000	348.0	6.08E-20	1.000	349.0	6.00E-20	1.000	350.0	5.53E-20	1.000
351.0	5.03E-20	1.000	352.0	4.50E-20	1.000	353.0	4.03E-20	1.000	354.0	3.75E-20	1.000	355.0	3.55E-20	1.000
356.0	3.45E-20	1.000	357.0	3.46E-20	1.000	358.0	3.49E-20	1.000	359.0	3.41E-20	1.000	360.0	3.23E-20	1.000
361.0	2.95E-20	1.000	362.0	2.81E-20	1.000	363.0	2.91E-20	1.000	364.0	3.25E-20	1.000	365.0	3.54E-20	1.000
366.0	3.30E-20	1.000	367.0	2.78E-20	1.000	368.0	2.15E-20	1.000	369.0	1.59E-20	1.000	370.0	1.19E-20	1.000
371.0	8.99E-21	1.000	372.0	7.22E-21	1.000	373.0	5.86E-21	1.000	374.0	4.69E-21	1.000	375.0	3.72E-21	1.000
376.0	3.57E-21	1.000	377.0	3.55E-21	1.000	378.0	2.83E-21	1.000	379.0	1.69E-21	1.000	380.0	8.29E-24	1.000
381.0	0.00E+00	1.000												

Table A-4. Values of chamber-dependent parameters used in the model simulations of the experiments for this study. [a]

Parm.	Value(s)	Discussion
k(1)	0.222 min ⁻¹	Derived by fitting results of quartz tube NO ₂ actinometry measurements to curve similar to that derived for other blacklight chambers by Carter et al (1995b). The results of the actinometry experiments carried out during this study were within the uncertainty range of this extrapolation.
k(O3W)	1.5x10 ⁻⁴ min ⁻¹	The results of the O ₃ dark decay experiments in this chamber are consistent with the recommended default of Carter et al (1995b) for Teflon bag chambers in general.
k(N25I) k(N25S)	2.8 x10 ⁻³ min ⁻¹ , 1.5x10 ⁻⁶ - k _g ppm ⁻¹ min ⁻¹	Based on the N ₂ O ₅ decay rate measurements in a similar chamber reported by Tuazon et al. (1983). Although we previously estimated there rate constants were lower in the larger Teflon bag chambers (Carter and Lurmann, 1990, 1991), we now consider it more reasonable to use the same rate constants for all such chambers (Carter et al., 1995b).
k(NO2W) yHONO	1.6x10 ⁻⁴ min ⁻¹ 0.2	Based on dark NO ₂ decay and HONO formation measured in a similar chamber by Pitts et al. (1984). Assumed to be the same in all Teflon bag chambers (Carter et al, 1995b).
k(XSHC)	250 min ⁻¹	Estimated by modeling pure air irradiations. Not an important parameter affecting model predictions except for pure air or NO _x -air runs.
RS/K1	3.27x10 ⁶ e ^{-7297/T} ppm	Based on model simulations of n-butane - NO _x experiments. The temperature dependence is derived from simulating outdoor experiments as discussed by Carter et al. (1995b).
E-NO2/K1	0.03 ppb	Based on model simulations of pure air experiments.

[a] See Table A-2 for definitions of the parameters.